








## Open Archive TOULOUSE Archive Ouverte (OATAO)

OATAO is an open access repository that collects the work of some Toulouse researchers and makes it freely available over the web where possible.

This is an author's version published in : <http://oatao.univ-toulouse.fr/19840>

**Official URL :** <https://dx.doi.org/10.2138/am-2018-6415>

### To cite this version :

Drouet, Christophe  and Aufray, Maëlen  and Rollin-Martinet, Sabrina and Vandecandelaere, Nicolas  and Grossin, David  and Rossignol, Fabrice and Champion, Eric and Navrotsky, Alexandra and Rey, Christian  *Nanocrystalline apatites: The fundamental role of water.* (2018) American Mineralogist, vol. 103 (n° 4). pp. 550-564.  
ISSN 0003-004X

Any correspondence concerning this service should be sent to the repository administrator :  
[tech-oatao@listes-diff.inp-toulouse.fr](mailto:tech-oatao@listes-diff.inp-toulouse.fr)

# Nanocrystalline apatites: The fundamental role of water

CHRISTOPHE DROUET<sup>1,\*†</sup>, MAËLENN AUFRAY<sup>1</sup>, SABRINA ROLLIN-MARTINET<sup>1,2</sup>,  
NICOLAS VANDECANDELAÈRE<sup>1</sup>, DAVID GROSSIN<sup>1</sup>, FABRICE ROSSIGNOL<sup>2</sup>, ERIC CHAMPION<sup>2</sup>,  
ALEXANDRA NAVROTSKY<sup>3</sup>, AND CHRISTIAN REY<sup>1</sup>

<sup>1</sup>CIRIMAT, Université de Toulouse, UMR CNRS/INPT/UPS 5085, ENSIACET, 4 allée Emile Monso, 31030 Toulouse cedex 4, France

<sup>2</sup>Université de Limoges, CNRS, SPCTS, UMR 7315, Centre Européen de la Céramique, 12 rue Atlantis, 87068 Limoges cedex, France

<sup>3</sup>Peter A. Rock Thermochemistry Laboratory and NEAT ORU, University of California Davis, 1 Shields Avenue, Davis, California 95616, U.S.A.

## ABSTRACT

Bone is a natural nanocomposite. Its mineral component is nanocrystalline calcium phosphate apatite, whose synthetic biomimetic analogs can be prepared by wet chemistry. The initially formed crystals, whether biological or synthetic, exhibit very peculiar physicochemical features. In particular, they are nanocrystalline, nonstoichiometric, and hydrated. The surface of the nanocrystals is covered by a non-apatitic hydrated layer containing mobile ions, which may explain their exceptional surface reactivity. For their precipitation *in vivo* or *in vitro*, for their evolution in solution, for the 3D organization of the nanocrystals, and for their consolidation to obtain bulk ceramic materials, water appears to be a central component that has not received much attention. In this mini-review, we explore these key roles of water on the basis of physicochemical and thermodynamic data obtained by complementary tools including FTIR, XRD, ion titrations, oxide melt solution calorimetry, and cryo-FEG-SEM. We also report new data obtained by DSC, aiming to explore the types of water molecules associated with the nanocrystals. These data support the existence of two main types of water molecules associated with the nanocrystals, with different characteristics and probably different roles and functions. These findings improve our understanding of the behavior of bioinspired apatite-based systems for biomedicine and also of biomineralization processes taking place *in vivo*, at present and in the geologic past. This paper is thus intended to give an overview of the specificities of apatite nanocrystals and their close relationship with water.

**Keywords:** Nanocrystalline apatite, water, hydroxyapatite, bone, DSC, cryo SEM, thermodynamics, enthalpy; Biomaterials—Mineralogy Meets Medicine

## INTRODUCTION

Nanocrystalline apatites constitute the mineral portion of bone and dentin (Gomez-Morales et al. 2013; LeGeros and LeGeros 1984). In these biominerals, nanocrystals are composed of a crystalline core of nonstoichiometric calcium phosphate apatite, deriving from hydroxyapatite  $\text{Ca}_{10}(\text{PO}_4)_6(\text{OH})_2$  and containing trace amounts of other mineral ions such as sodium, strontium, fluoride, etc. This core is covered by a non-apatitic ionic hydrated layer (Cazalbou et al. 2004a; Eichert et al. 2005, 2008; Jäger et al. 2006; Rey et al. 1989, 1990, 2007; Grossin et al. 2010; Vandecandelaere et al. 2012; Gomez-Morales et al. 2013; Wang et al. 2013), conferring exceptional surface reactivity that is exploited *in vivo* for regulating ionic concentrations in body fluids in homeostasis processes (Bonjour 2011; Rey et al. 1989, 1990, 2009; Driessens et al. 1986). The overall composition of bone apatite can generally be satisfactorily described as  $\text{Ca}_{10-x}(\text{PO}_4)_{6-x}(\text{HPO}_4)_x(\text{CO}_3)_x(\text{OH}, \frac{1}{2}\text{CO}_3)_{2-x}$  with  $0 \leq x \leq 2$  (Eichert et al. 2007; Rey et al. 2009), and compilation of cortical bone analyses suggested the following averaged chemical composition

(Legros et al. 1987):  $\text{Ca}_{8.3}(\text{PO}_4)_{4.3}(\text{HPO}_4)_1.7(\text{OH}, \frac{1}{2}\text{CO}_3)_{0.3}$ . In these formulas, carbonation can be present by substitution of hydroxyl groups in the so-called apatitic-channels of the lattice (A-type carbonates) or of phosphate groups (B-type). Labile carbonate (LC) species corresponding to surface carbonate ions within the surface layer can also be identified. The overall degree of carbonation is low for early, immature apatitic deposits, but it progressively increases up to several weight percent upon aging. For charge compensation, some  $\text{PO}_4^{3-}$  ions are substituted by  $\text{HPO}_4^{2-}$  ions (which, in the apatitic lattice, occupy the same type of sites as B-type carbonates).

It is possible to prepare biomimetic analogs to bone apatite, either carbonate-substituted or non-carbonated, by soft chemistry using close-to-physiological synthesis routes such as coprecipitation (Delgado-Lopez et al. 2012; Iafisco et al. 2011, 2012; Vandecandelaere et al. 2012; Pasteris et al. 2012). These synthetic compounds not only help us to understand biomineralization phenomena, but also encourage the development of bio-inspired materials for bone regeneration and, more recently, in nanomedicine, e.g., for oncology (Drouet et al. 2015; Kramer et al. 2014; Iafisco et al. 2012, 2013; Bouladjine et al. 2009), gene delivery (Hossain et al. 2010; Sokolova et al. 2006; Chowdhury and Akaike 2005) and hematology (Stefanic et al. 2017). For

\* E-mail: christophe.drouet@cirimat.fr

such applications, raw precipitates must be processed into either 3D scaffolds, 2D surface coatings on appropriate substrates, or even 1D individualized nanoparticles; this processing step may lead to non-negligible modifications of the initial nanocrystals.

Whether for synthesis by precipitation in aqueous solution, nanocrystal evolution in solution or in natural bone environment *in vivo*, or biomaterials processing (potentially involving drying, consolidation, and sterilization steps), one actor remains ubiquitous: water. This component indeed appears as a major ingredient for deciphering apatite nanocrystal formation and fate in humid conditions. However, to date, focus has rarely been placed on this “constituent of life” from a physicochemical point of view when dealing with apatite.

In such nonstoichiometric apatite compounds, water molecules could possibly occupy several sites: on the surface of the crystals (within the hydrated ionic layer), but also possibly in some ion vacancies in the lattice (vacancies in OH sites, in calcium sites, or in the oxygen vacancy left in phosphate sites by the  $\text{CO}_3$ -for- $\text{PO}_4$  substitution in the case of B-type carbonate). Figure 1 shows in a schematic way the possible positions of ion vacancies in the apatite lattice. Neuman and Neuman (1953) and Neuman et al. (1953) discussed the hydration state of bone and synthetic apatite, and mentioned that “the water associated with the crystals of both synthetic hydroxyl apatite and bone when in aqueous media does not appear to be due either to capillary condensation or to the formation of a crystalline hydrate,” thus suggesting a different involvement of water molecules, although they concluded that “the concept of the hydration shell requires considerable clarification.” In his review, Glimcher (1959) pointed out for precipitated apatites the presence of “excess water [that] cannot be separated from the crystals by mechanical centrifugation at 80 000 g,” later referring to water being part of “a large hydration shell of water ‘bound’ to the crystals,” and concluded by adding: “the very large surface tension and capillarity effects between such crystal surfaces could well ‘trap’ a large amount of water in addition to a bound monolayer, and still resist separation from the crystals by mechanical centrifugation.” These conclusions underlined the ubiquitous presence of water, although no clarification of the type of interactions with the

mineral was presented. By way of birefringence measurements at various temperatures from 60 to 400 °C for 2 h periods, Carlström et al. (1963) examined the water bound to enamel and concluded the existence of two different types: one “very loosely bound” that they attributed to the organic matrix and a larger part “firmly bound to the mineral phase.” However no details were given on the water specifically linked to the mineral. Also that report dealt with relatively large enamel crystals, closer to stoichiometric hydroxyapatite than bone crystals. In bone, Timmins and Wall (1977) reported a review on the presence of water associated more or less strongly with the tissue, but no experimental data were given for the water related to the mineral phase. LeGeros et al. (1978) reported some data for water associated to enamel and precipitated apatites, for which they pointed out two types of associated water, referred to as “adsorbed” and “lattice” water, released sequentially upon heating. The latter authors considered the “adsorbed” water as of the water type previously considered by Carlström as linked to the organic matrix, and they attributed the “lattice” water to “ $\text{H}_2\text{O}$ -for-OH” and/or “ $\text{HPO}_4$ -for- $\text{PO}_4$ ” substitutions in the apatitic lattice. Taking into account their heating conditions (to 400 °C at 5 °C/min), the decomposition of  $\text{HPO}_4^{2-}$  ions from the lattice is indeed expected to generate  $\text{H}_2\text{O}$  molecules either in condensation to form pyrophosphate ( $\text{P}_2\text{O}_7^{4-}$ ) ions or in reaction with carbonate ions to give  $\text{CO}_2$  and  $\text{H}_2\text{O}$ . However, again, little is known about the water initially present (not formed upon decomposition of other chemical species). Starting in 2006, cold sintering (e.g., spark plasma sintering) was applied to nanocrystalline apatites (Drouet et al. 2006, 2009; Grossin et al. 2010), pointing out the possibility to consolidate these compounds at low temperature, typically around 150 °C. To explain this possibility despite a low thermal activation of ion diffusion in these conditions, the role of the hydrated layer, and thus of water, was then evidenced for the first time. Indeed, a high mobility of the ions contained in surface hydrated environments is thought to allow ion diffusion and therefore to favor crystal-crystal interactions despite the low temperature. Rollin-Martinet (2011) realized cryo-FEG-SEM analyses of synthetic apatite nanocrystals during the precipitation stage, unveiling the formation of bundles of aligned nanocrystals surrounded by a

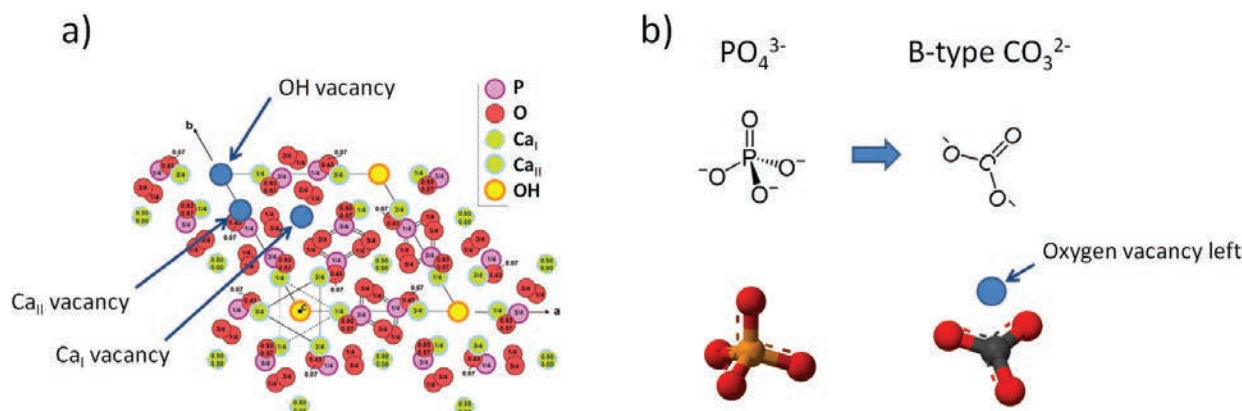


**FIGURE 1.** Possible position of vacancies in the apatite lattice, where some water molecules could potentially reside (beside the water contained within the surface hydrated layer on the nanocrystals): (a) vacancies in  $\text{OH}^-$  (on the axis of apatitic channels) and  $\text{Ca}^{2+}$  sites ( $\text{Ca}_\text{I}$  and  $\text{Ca}_\text{II}$ ) represented on the basis of the hydroxyapatite crystal lattice, (b) oxygen vacancy left in the case of  $\text{CO}_3$ -for- $\text{PO}_4$  substitution (B-type carbonate). In this schematic representation, no distortion of the  $\text{PO}_4$  tetrahedron nor of the  $\text{CO}_3$  plane are shown. (Color online.)

seemingly amorphous shell suspected to be water rich. Wang et al. (2013) reported a similar role of water in the orientation of apatite crystals in bone tissue. They also concluded that “structuring water molecules strongly interact with the mineral when a disordered mineral layer coats the crystalline core of the mineral particles.” This statement parallels the conclusions drawn from low-temperature sintering experiments; indeed, in both cases (in bone and for the consolidation of nanocrystalline apatites), the organization of the nanocrystals is linked to (controlled by?) the hydrated layer present on the nanocrystals. Also, the “disordered mineral layer” corresponds perfectly to the hydrated and ionic surface layer present on the nanocrystals previously reported (Vandecandelaere et al. 2012; Káflak and Kolodziejski 2008; Cazalbou et al. 2004a, 2004b; Lu et al. 2000; Rey et al. 1989, 1990; Roufosse et al. 1984). Granke et al. (2015) explored the mechanical behavior of bone and related it to its water content to complement other works on this topic (Unal and Akkus 2015; Nyman et al. 2006). In addition, Nyman et al. (2008) developed an NMR-based methodology to follow the “mobile” and “bound” water associated with human femurs; where “mobile” water is considered to fill microscopic pores (found in Haversian canals, canaliculi, and lacunae) while “bound water” refers to a “structural water layer bridging mineral and collagen.” The eventuality of different types of water molecules was also reported by Wilson et al. (2005, 2006) from NMR experiments, where water was suspected to “occupy the vacancies created by substitutions and defects in the crystal lattice” but also to be involved in more superficial chemical environments for mediating mineral-organic matrix interactions. Yoder et al. (2012a, 2012b) and Pasteris et al. (2014), reported NMR, TGA, and Raman spectroscopy data on carbonated apatites and interpreted them by considering that water molecules resided in apatite channels, although no direct correlation was found in these works between the density of vacancies and the amount of water incorporated in the apatite lattice. In older works, using essentially TGA, LeGeros et al. (1979) and Labarthe et al. (1973) reported also on water trapped in the lattice of type B carbonated apatites, considered to be associated with oxygen vacancies in sodium-free carbonated apatites but independent of the carbonate content in sodium-containing carbonated apatites as confirmed by Pasteris et al. (2014). The presence of incorporated water in nonstoichiometric apatites has also been proposed on the basis of Rietveld refinement of XRD data as in Ivanova et al. (2001), either in apatite channels or in replacement of the oxygen vacancy left by substituting  $\text{PO}_4$  by  $\text{CO}_3$ .

As can be seen from the above, water appears strongly involved in mineralized tissues, including substantial interaction with the mineral component, although several conceptions have been expressed along the years (water associated to the organic component, water in porosity, water from the hydrated layer, adsorbed water, water in OH vacancies or in calcium vacancies or in the oxygen vacancies in the lattice, ...), as summarized chronologically by Pasteris (2012). Today, the water-mineral system requires specific attention more than ever, with consideration of several complementary aspects involving water and apatite nanocrystals. In the present mini-review, we wish to give water the central role it deserves, by providing a global picture of the fundamental role that it plays in the genesis, evolution, and

interaction schemes involving apatite nanocrystals. For easier reading, the text is divided into several successive subsections referring to the synthesis of the nanocrystals and their evolution in solution (including thermodynamic aspects), the impact of drying, the exploration of the different “types” of water molecules associated with the nanocrystals, the role of water in the 3D organization of the nanocrystals, their consolidation at “low” temperature by cold sintering to obtain bioceramics, and finally some considerations relevant to the *in vivo* setting.

## MATERIALS AND METHODS

Biomimetic apatite samples were produced and characterized by TEM, FTIR, XRD, and TGA as described previously (Vandecandelaere et al. 2012).

Differential scanning calorimetry (DSC) was performed using a DSC 204 Phoenix Series (Netzsch, Selb, Germany) coupled with a TASC 414/4 controller. The apparatus was calibrated against melting temperatures of In, Hg, Sn, Bi, CsCl, and Zn, applying two 10 °C/min temperature ramps, as recommended (Della Gatta et al. 2006). The calibration was verified before each experiment using indium, with an accuracy of  $\pm 0.5$  °C and  $\pm 0.5$  J/g. The samples were placed in stainless steel capsules (120  $\mu\text{L}$ ) and the mass was measured with an accuracy of  $\pm 0.1$  mg. The samples were heated from  $-50$  to  $300$  °C at  $10$  °C/min under a continuous flow of nitrogen.

A field emission gun scanning electron microscope (JEOL 7400) equipped with a cryogenic system (Gatan Alto 2500), or “Cryo-FEG-SEM,” was used to examine the morphology of freshly precipitated, wet apatite nanocrystals at various time points during their maturation in solution. For each analysis, one droplet was sampled with a pipette out of the precipitating medium and deposited on the sample holder. The system was then frozen and transferred into a chamber cooled with liquid nitrogen.

Technical details on the consolidation of nanocrystalline apatites by cold sintering and related mechanical testing were reported by Grossin et al. (2010). The relative density of the samples was calculated from the ratio between their apparent density (evaluated from the dimensions of the consolidated cylindrical pellets and their mass) and their true density (determined by He pycnometry with a Micromeritics AccuPyc 1330 apparatus, with 10 successive measurements on each sample).

Ion exchange was carried out by immersing 200 mg of nanocrystalline apatite sample in 50 mL of a 1 M aqueous solution of magnesium chloride  $\text{MgCl}_2 \cdot 6\text{H}_2\text{O}$ , at room temperature under stirring, for 30 min. The suspension was then filtered, washed with deionized water and freeze-dried. Ca and Mg concentrations were then determined by ICP-AES analyses (uncertainty on alkaline-earth titration: 5%).

High-temperature oxide melt calorimetry was carried out in a Tian-Calvet twin calorimeter, as previously described (Rollin-Martin et al. 2013; Ushakov et al. 2001). A minimum of 8 values were obtained for each composition, and uncertainties are 2 st. dev. of the mean.

## RESULTS AND DISCUSSION

### Synthesis of nanocrystalline apatites via wet chemistry

Apatite samples precipitated at moderate temperature, typically under the boiling point of the solution, generally exhibit a nonstoichiometric chemical composition, with less calcium and hydroxide than the theoretical hydroxyapatite (HAP) formula  $\text{Ca}_{10}(\text{PO}_4)_6(\text{OH})_2$  (Gomez-Morales et al. 2013; LeGeros and LeGeros 1984). Although the preparation of stoichiometric HAP in the dry state can be done easily by calcining in (moist) air various reactants used in stoichiometric proportions, e.g., by mixing  $\text{CaCO}_3$  and  $\beta$  tricalcium phosphate  $\text{Ca}_3(\text{PO}_4)_2$  (Elliott 1994), obtaining truly stoichiometric HAP from wet chemistry is a delicate process as calcium and hydroxide crystallographic sites need to be completely filled. This is generally realized at (or close to) boiling temperature, under alkaline pH, and usually via dropwise addition of the calcium and phosphate reactants under constant stirring (Raynaud et al. 2002). Therefore, many wet syntheses of apatite—especially in mild conditions close to



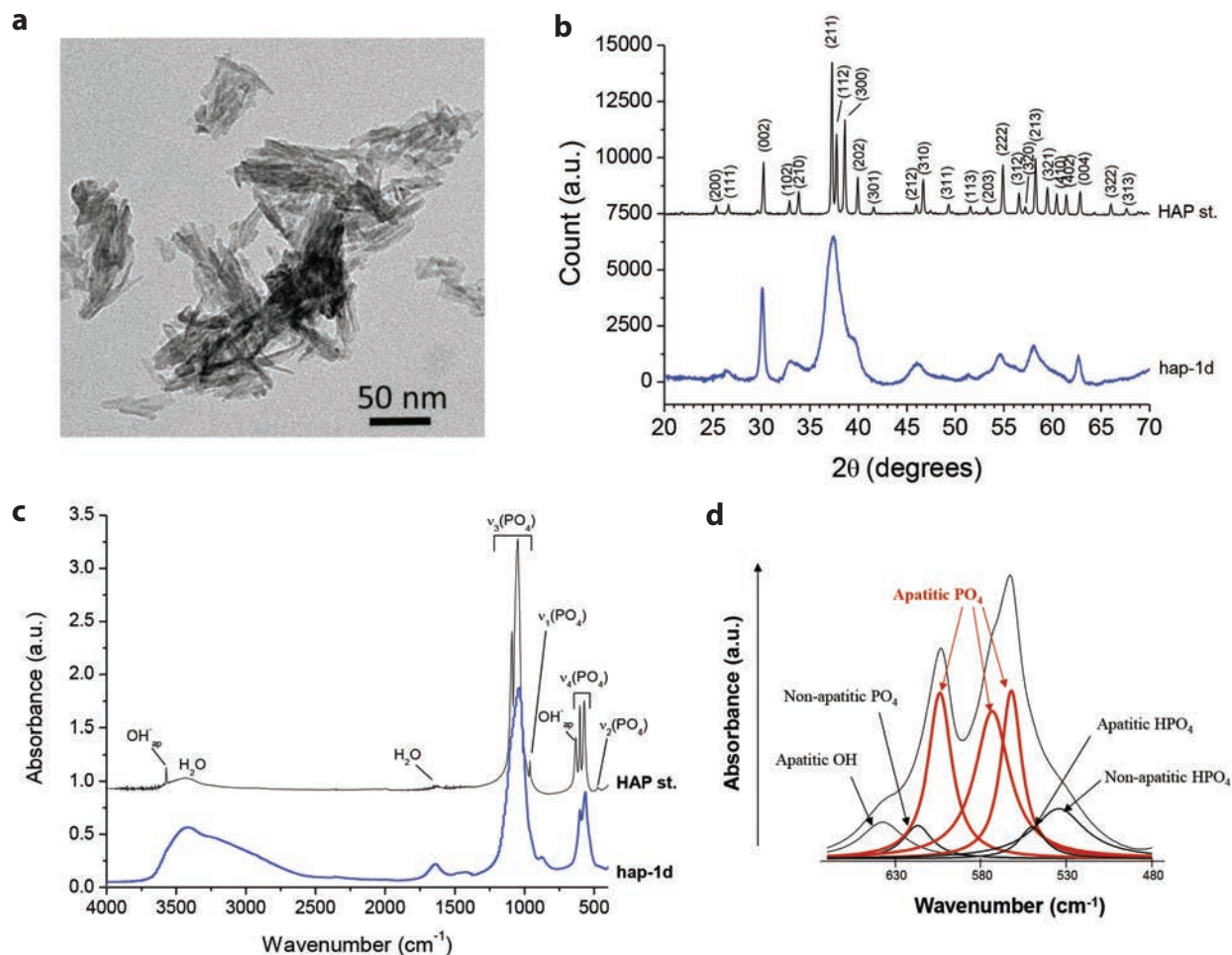


**FIGURE 2.** Typical characteristics of biomimetic nanocrystalline apatites [e.g., matured 1 day (a, b, c) or 3 weeks (d)] and of stoichiometric HAP sintered at 1000 °C<sup>-1</sup> h (b and c). (a) TEM micrograph, (b) XRD pattern ( $\lambda_{\text{cobalt}} = 1.78892 \text{ \AA}$ ), (c) FTIR spectra, and (d) detail on the  $\nu_4(\text{PO}_4)$  FTIR spectral domain. (Color online.)

physiological—produce nonstoichiometric compositions. This is the case in bone *in vivo* and also in the preparation of biomimetic analogs (Vandecastelaere et al. 2012). For instance, chemical titrations for an apatite matured 1 day at 22 °C and pH 7.2 (prior to filtration and freeze-drying) resulted in the mean composition  $\text{Ca}_{8.64}(\text{PO}_4)_{4.88}(\text{HPO}_4)_{1.12}(\text{OH})_{0.39}$ , corresponding to a Ca/P molar ratio of  $1.44 \pm 0.02$ , significantly lower than the value of 1.67 for stoichiometric HAP. An example of samples precipitated at 22 °C is given in Figure 2. TEM observation (Fig. 2a) confirms the nanometric dimensions of the constitutive crystals, and shows an elongated crystal shape with a tendency to form platelets. X-ray diffraction (XRD) analysis reveals (Fig. 2b) the low intensity and large FWHM of the peaks when compared to well-crystallized stoichiometric HAP (Vandecastelaere et al. 2012; Grynpas 1976). This low crystallinity can be attributed both to the nanometric size of the crystals and to the existence of internal crystal strain due to nonstoichiometry and other point defects in the crystal. Additionally, Fourier transform infrared (FTIR) spectroscopy of biomimetic nanocrystalline apatite detects (Fig. 2c) not only the characteristic vibrations of calcium phosphate

apatite, but also an enhanced contribution of water molecules, as evidenced by a broad band in the range 2700–3500  $\text{cm}^{-1}$  assignable to O-H stretching in  $\text{H}_2\text{O}$ , as well as an increase of the HOH bending contribution of water at 1640  $\text{cm}^{-1}$ . Moreover, as for bone apatite (Rey et al. 1990), other spectral features differ from those of well-crystallized stoichiometric HAP. This is particularly visible in the  $\nu_4(\text{PO}_4)$  spectral domain where, in addition to the libration band of apatitic  $\text{OH}^-$  ions around 632  $\text{cm}^{-1}$  and the three typical contributions of apatitic  $\text{PO}_4^{3-}$  groups (around 601, 575, and 560  $\text{cm}^{-1}$ , marked in red on Fig. 2d), other bands are also clearly detectable in biomimetic apatites: at lower wavenumbers [attributed to  $\text{HPO}_4$  vibrations in either “apatitic” (~550  $\text{cm}^{-1}$ ) or “non-apatitic” (534  $\text{cm}^{-1}$ ) chemical environments], and at high wavenumbers (around 617  $\text{cm}^{-1}$ , assigned to “non-apatitic”  $\text{PO}_4^{3-}$  ions). Details of the vibrational spectroscopy features have been reported elsewhere (Rey et al. 2014b) and peak assignments in biomimetic apatites have been specifically discussed in a previous study (Vandecastelaere et al. 2012). While the “apatitic” domains refer to ions located in regular apatite crystallographic sites, “non-apatitic” environments refer to ionic locations that

do not correspond to positions within the hydroxyapatite lattice. The latter are located on the surface of the nanocrystals where they are associated with water and form a non-apatitic hydrated ionic layer (Eichert et al. 2005; Rey et al. 2014a).

Therefore, several physicochemical features differ significantly between stoichiometric HAP and nanocrystalline biomimetic apatites: (1) the latter are constituted of nanosized crystals, (2) they are nonstoichiometric with vacancies in the calcium and hydroxide sites and contain  $\text{HPO}_4^{2-}$  ions (partly replaced by  $\text{CO}_3^{2-}$  ions in bone or in synthetic carbonated analogs), (3) they exhibit an elongated/platelet crystal shape, and (4) they expose a non-apatitic hydrated ionic layer on their surface. These phenomena represent the four leading conditions defining “biomimetic” or “bone-like” apatite samples. Since these systems are composed of “nano” and “hydrated” crystals, the use of high temperatures (e.g., approaching or beyond the boiling point of the solution), especially for extended periods should be avoided to obtain/preserve biomimetic apatite compounds. Consequently, synthesis routes involving at least one wet-chemistry step are central.

### Hydrated surface layer

As a part of the surface layer, water molecules appear as a key component during crystal genesis. The formation of a hydroxyapatite  $\text{Ca}_{10}(\text{PO}_4)_6(\text{OH})_2$  crystallographic unit cell (hexagonal system, space group  $P6_3/m$ ,  $Z = 1$ ) involves 44 atoms distributed in the form of 18 ions. Organization of all these ions to elaborate a crystal is thus bound to take time, especially at “low” temperature (e.g., at room or physiological temperature) and under atmospheric pressure. We believe that the hydrated ionic layer on the surface of the nanocrystals might be seen as a “remnant” of the apatite growth process in solution. At neutral/physiological pH, the speciation of phosphate ions clearly favors protonated forms ( $\text{HPO}_4^{2-}/\text{H}_2\text{PO}_4^-$ ) over the deprotonated form  $\text{PO}_4^{3-}$ , which essentially does not exist in these conditions (see phosphoric acid speciation diagram, e.g., Luong and Liu 2017). Apatite is however quite insoluble [solubility product  $\sim 10^{-58}$  for stoichiometric hydroxyapatite  $\text{Ca}_{10}(\text{PO}_4)_6(\text{OH})_2$ , Chander and Fuerstenau 1984; Elliott 1994]; therefore formation of this calcium phosphate phase can occur even at pH values where only a small amount of phosphate ions  $\text{PO}_4^{3-}$  is available because the activity product of the ions involved in the apatite precipitation equilibrium ( $\text{Ca}^{2+}$ ,  $\text{PO}_4^{3-}$ ,  $\text{OH}^-$ ) exceeds the solubility product. In (close-to) physiological conditions, it is not surprising that initial phosphate incorporation upon precipitation may involve protonated phosphate ions, and  $\text{HPO}_4^{2-}$  ions are indeed clearly detected by FTIR especially in surface “non-apatitic” environments (see Fig. 2d). Some recent papers have introduced the concept of prenucleation clusters involving  $\text{Ca}^{2+}$  and  $\text{HPO}_4^{2-}$  ions (Mancardi et al. 2016; Habraken et al. 2013) forming before nucleation. Although experimental evidence for such clusters is difficult to obtain, there is at least a consensus on the strong involvement of protonated phosphate ions at the early stages of apatite nanocrystal formation. In contrast, in the crystal core, deprotonated phosphates become more abundant to approach the HAP composition.

The crystal surface probably cannot be described as a sharp interface between the solid and the solution (Fig. 3I), but instead as an *interphase* that could be visualized as an extended surface

domain progressively allowing the “transition” from the solution to the crystal core as illustrated on Figure 3II). Solid-state NMR data (recorded on dried samples) seem to support this assessment, revealing that the surface layer of moderately mature apatite samples reaches a depth on the nanometer scale (Jäger et al. 2006). When apatite nanocrystals are in contact with solution, three components coexist: the solution, the hydrated layer, and the apatite crystal core. The surface layer belongs to the crystal, even after freeze-drying, as shown in Figures 1c and 1d. This *interphase* involves two “interfaces” (Fig. 3III): a first one between the solution and the hydrated ionic layer, and a second deeper interface between the surface layer and the crystal core itself. Two-dimensional solid-state NMR (Wang et al. 2012; Rey et al. 2007; Sfihi and Rey 2002) pointed out correlations through heteronuclear dipolar interaction (for example via  $^1\text{H} \rightarrow ^{31}\text{P}$  HetCor experiments), allowing to distinguish NMR-active nuclei that are spatially close to each other. On the one hand, apatitic species like apatitic phosphates and carbonates contained in the crystal core and apatitic  $\text{OH}^-$  ions correlated with each other. On the other hand, non-apatitic species correlated with each other; indeed non-apatitic (hydrogen) phosphate and labile carbonate species correlated with water molecules. These findings indicate that non-apatitic species are localized in a separate domain as apatitic ones, thus corroborating the “hydrated layer model” already proposed on the basis of vibrational spectroscopy data. It should be emphasized that although XRD data do not provide structural information on the surface layer, which is thin and appears “amorphous-like” in the dry state, some degree of organization exists within this layer. Indeed, the spectral signatures of non-apatitic ionic species (e.g.,  $\text{HPO}_4^{2-}$  ions,  $\text{PO}_4^{3-}$  ions), whether analyzed by FTIR, Raman, or NMR, systematically fall at the same positions, suggesting some constancy of chemical environments in synthetic samples and in bone crystals.

### The concept of maturation in solution

This surface layer should not be considered as a “simple” hydration layer solely made of water molecules, nor as a Stern electrical double layer, referring to the accumulation of ions and counter-ions from the solution in the form of a double layer on the surface of a solid (Grahame 1947). Instead, on apatite nanocrystals, this layer contains water closely associated with ions located in chemical environments (Fig. 3IV) that lead to very specific spectroscopic signatures (see for example Fig. 2d). Upon “maturation,” ions gradually fill crystallographic positions corresponding to the apatitic lattice (Figs. 3IV to 3VI).

The concept of maturation can be investigated experimentally by analyzing apatites left in the precipitating medium for an increasing period of time prior to filtration, washing and (freeze)drying. In carbonate-free conditions, the effect of maturation has been explored in detail (Vandecastelaere et al. 2012). Figure 4 shows variables of crystal evolution vs. the maturation time, quantified by the Ca/P molar ratio of the precipitate, the overall XRD pattern, as well as the mean crystallite dimensions estimated using Scherrer’s formula. The physicochemical characteristics of the solid evolve upon aging in solution: (1) the Ca/P ratio increases, indicating an evolution toward HAP stoichiometry (although not reaching it in these conditions), (2) XRD patterns progressively show increasing crystallinity, and



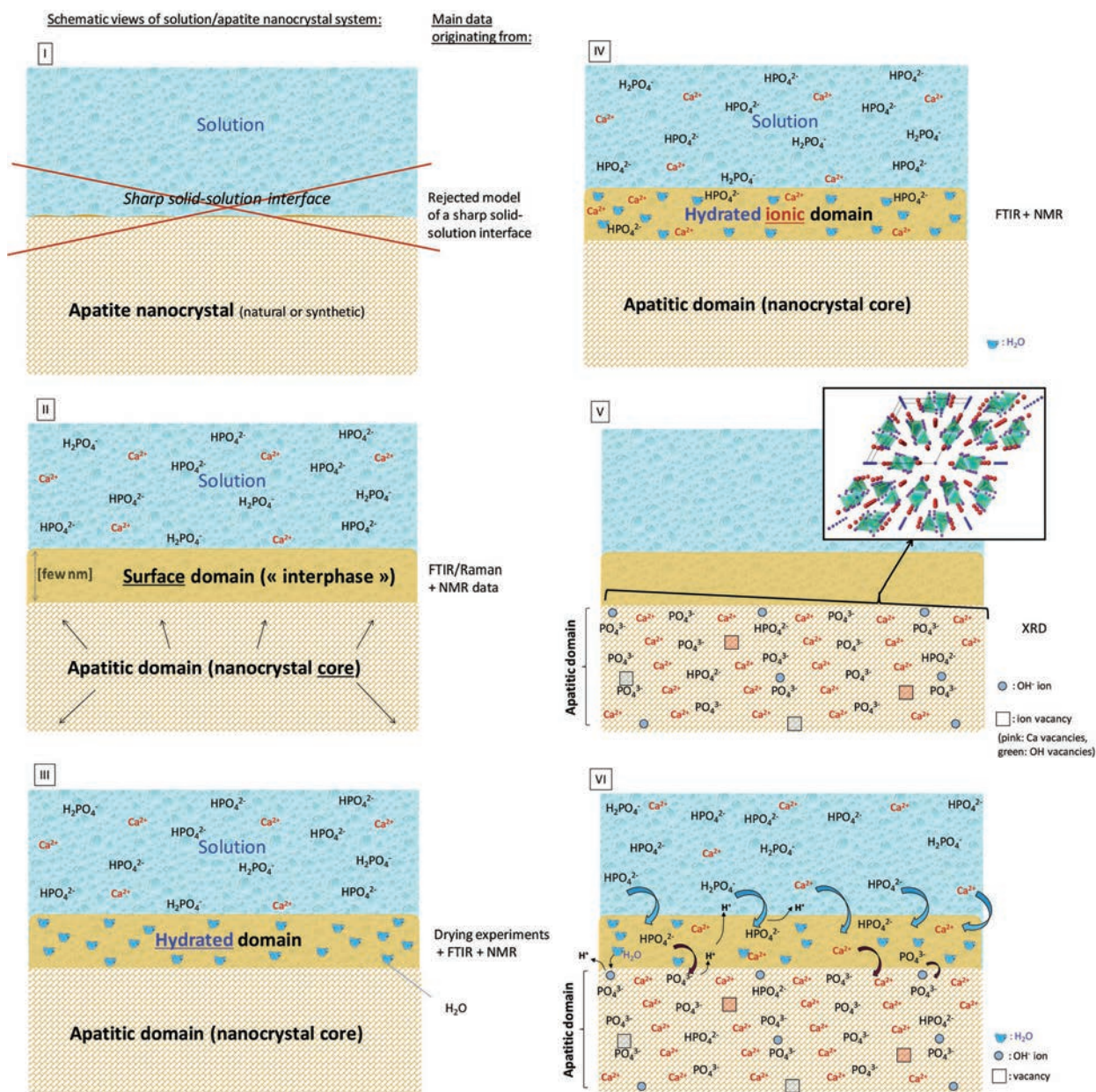
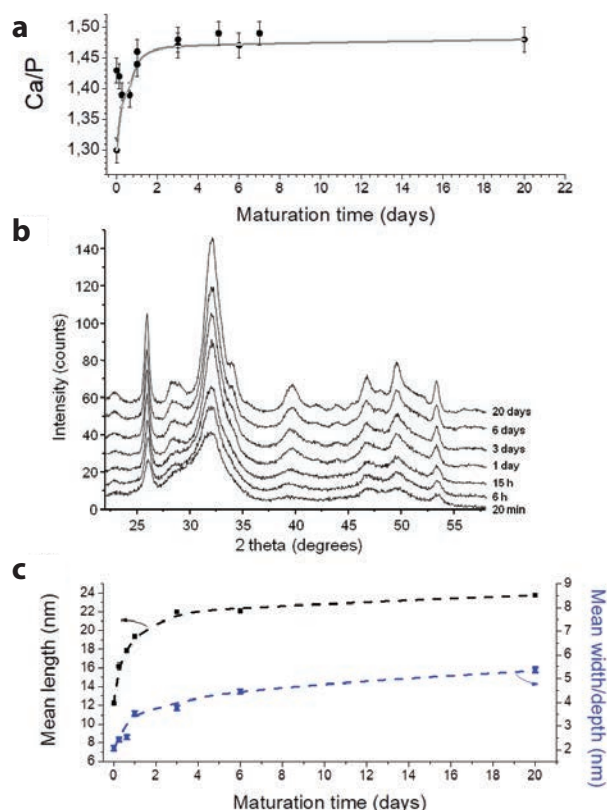


FIGURE 3. Schematic representation of an apatite nanocrystal in contact with an aqueous medium (carbonate-free conditions). (Color online.)

(3) mean crystallite dimensions systematically increase. These modifications indicate a continuous progression of the crystallization process over the time spent in wet conditions. More in-depth examination of the ionic contents upon maturation also shows that the amount of non-apatitic chemical environments and of overall associated water (followed by TGA) decrease, while the apatitic OH<sup>-</sup> content increases (Fig. 5). These findings indicate that maturation favors the development of the crystalline core at the expense of the surface hydrated ionic layer (Fig. 3VI). It may be noted that the situation is somewhat different in the presence of carbonates: in this case, evolution toward stoichiometry and concomitant increase of OH<sup>-</sup> contents are less

noticeable; in contrast a clear increase of carbonation is noticed upon maturation (Eichert 2001).

It is interesting to examine the maturation process in more detail, by considering the chemical species involved. As indicated above, in the case of carbonate-free samples an increase of the overall Ca/P ratio of the solid phase is observed experimentally. At the atomic/molecular level, this evolution could theoretically be explained either by an increased incorporation of calcium ions in the crystal lattice (increase of numerator), or by a release of phosphate ions (decrease of denominator). However, in physiological or physiological-like conditions corresponding to nanocrystalline apatite precipitation, the amount of free Ca<sup>2+</sup> ions in



**FIGURE 4.** Effect of apatite maturation in solution (at 22 °C) on (a) Ca/P molar ratio, (b) XRD pattern ( $\lambda_{\text{copper}} = 1.514 \text{ \AA}$ ), and (c) mean crystallite dimensions as estimated from Scherrer's formula. (Color online.)

solution remains very low (Drouet 2013) due to the presence of calcium-binding agents such as phosphates, carbonates, and proteins. Therefore, the increase of Ca/P may better be explained as a release of phosphate ions expelled from the solid phase during its progression toward stoichiometry (in carbonated conditions  $\text{CO}_3^{2-}$  ions get progressively incorporated). A proposed overall maturation scheme is represented schematically in Figure 6. Both calcium and phosphate ions from the hydrated layer progressively enter the apatitic core. Concerning phosphate, a larger incorporation of  $\text{PO}_4^{3-}$  ions rather than  $\text{HPO}_4^{2-}$  is expected in the hydroxyapatite structure;  $\text{PO}_4^{3-}$  arising from the deprotonation of  $\text{HPO}_4^{2-}$ , which simultaneously releases protons. Some  $\text{Ca}^{2+}$  ions are also incorporated to balance electrical charges. Remaining  $\text{HPO}_4^{2-}$  ions can then combine with the released protons to form monovalent  $\text{H}_2\text{PO}_4^-$  that leaves the crystal, accompanied by the excess of calcium ions. In parallel, a small amount of  $\text{OH}^-$  can also enter the apatitic core accompanied by calcium ions for preservation of the electroneutrality of the crystal, but this is not represented in Figure 6 for the sake of simplicity.

### The key role of thermodynamics

The chemical evolution undergone by apatite nanocrystals either in vivo or in biomimetic analogs appears inevitable as long as apatite nanocrystals are in humid conditions. To explore the thermodynamic basis of this process, oxide melt solution calorimetry has been performed on biomimetic apatites cor-

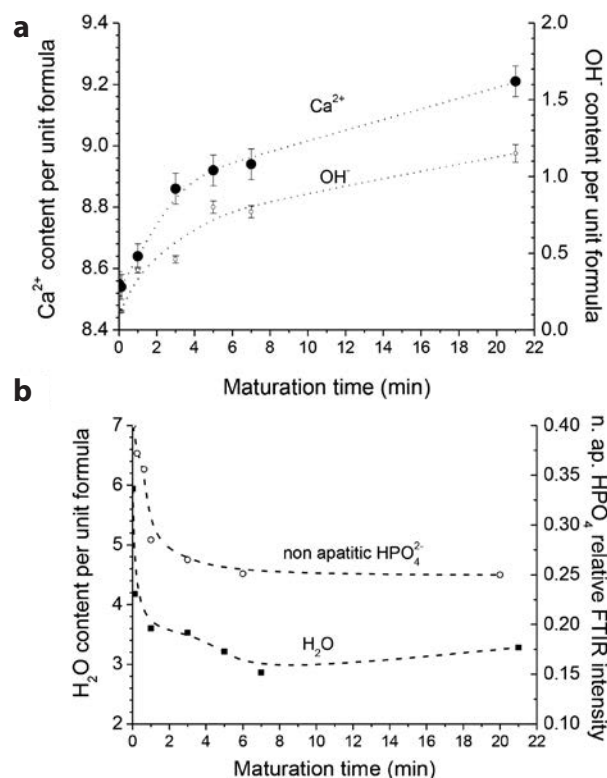


**FIGURE 5.** Evolution of ionic contents of nanocrystalline apatites vs. maturation (at 22 °C): (a)  $\text{Ca}^{2+}$  and  $\text{OH}^-$  contents per unit formula and (b) example of  $\text{H}_2\text{O}$  content per unit formula (as measured from TGA for one given set of batches freeze-dried for 3 days) and evolution of non-apatitic  $\text{HPO}_4^{2-}$  environments [in relative proportion from FTIR analysis of the  $\nu_4(\text{PO}_4)$  band: peak area ratio between n.ap.  $\text{HPO}_4$  band at  $534 \text{ cm}^{-1}$  and overall  $\nu_4(\text{PO}_4)$  band area].

### The maturation process from a chemical viewpoint:

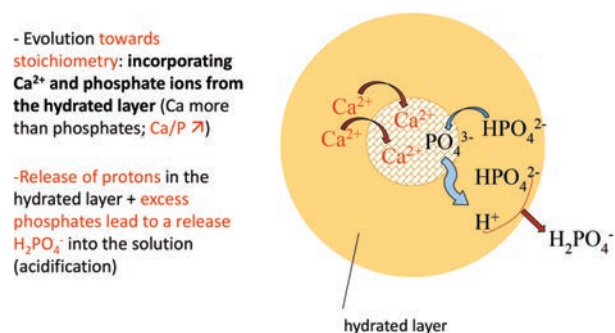


**FIGURE 6.** General scheme for apatite maturation in solution (carbonate-free conditions). (Color online.)

responding to increasing maturation times (Rollin-Martin et al. 2013). These measurements allowed determination of the corresponding standard enthalpy of formation  $\Delta H_f^\circ$  of the related apatite compounds via the use of an appropriate thermodynamic cycle. Results, reported in Table 1, show that the value of  $\Delta H_f^\circ$  for the anhydrous apatite samples (enthalpy of formation from



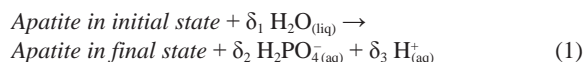
**TABLE 1.** Experimental  $\Delta H_{ds}$  values and derived  $\Delta H_{f,oxides}$ ,  $\Delta H_f^\circ$ , and  $\Delta G_f^\circ$  for nanocrystalline apatites with increasing maturation states

Sample	$\Delta H_{ds}$ (apatite, hydrated) (kJ/mol)	$\Delta H_f^\circ$ (apatite, hydrated) (kJ/mol)	$\Delta H_{f,oxides}$ (kJ/mol)	$\Delta H_f^\circ$ (apatites, anhydrous) (kJ/mol)	$\Delta G_f^\circ$ (kJ/mol)
<b>Nanocrystalline apatites</b>					
20 min	1197.7 ± 10.0 (10)	-13756.8 ± 12.2	-1952.2 ± 12.5	-12058.9 ± 12.2	-11323.1 ± 12.2
3 h	1198.2 ± 15.0 (9)	-13370.7 ± 16.5	-2073.9 ± 16.8	-12174.9 ± 16.5	-11439.7 ± 16.5
1 day	1241.7 ± 9.5 (8)	-13393.4 ± 11.8	-2152.7 ± 12.1	-12364.4 ± 11.8	-11616.0 ± 11.8
3 days	1088.6 ± 9.1 (9)	-13352.3 ± 11.5	-2032.8 ± 11.8	-12342.1 ± 11.5	-11595.0 ± 11.5
5 days	1077.4 ± 5.1 (9)	-13373.3 ± 8.7	-2030.5 ± 9.2	-12457.0 ± 8.7	-11692.6 ± 8.7
1 week	1137.2 ± 9.1 (10)	-13362.2 ± 11.5	-2119.5 ± 11.9	-12546.1 ± 11.5	-11783.9 ± 11.5
3 weeks	1172.8 ± 20.2 (9)	-13708.7 ± 21.4	-2141.3 ± 21.6	-12771.0 ± 21.4	-11994.2 ± 21.4
HAP st.	1027.7 ± 21.4 (11)	-13477 ± 10	-2283.5 ± 23.0	-13477 ± 10	-12674.2 ± 10

Note: Numbers in parentheses refer to the number of calorimetry experiments performed.

the elements in their standard state, at 298 K and 1 bar) becomes significantly more exothermic upon maturation: enthalpy change is thus associated with the maturation process.

Taking into account entropy estimations (Rollin-Martinet et al. 2013), it also becomes possible to evaluate the corresponding Gibbs free energy of formation  $\Delta G_f^\circ$ , which is also shown in Table 1. Again, a clear trend toward more negative values is seen, with a tendency to evolve toward stoichiometric hydroxy-apatite. These results thus indicate that the nanocrystals become increasingly stable as maturation progresses. Comparing the  $\Delta G_f^\circ$  values between more and less mature samples allows estimation of the Gibbs free energy accompanying the maturation process, denoted  $\Delta G_{maturation}$  (see below). For this task however, it is necessary also to take into account all the chemical species involved in the maturation process, including participating aqueous ions from the solution (thermodynamic data taken from reference literature sources Robie and Hemingway 1995 and Wagman et al. 1982). As discussed above and shown schematically in Figure 6, maturation is probably accompanied by a release of phosphate rather than an uptake of free  $Ca^{2+}$  ions. Considering the following simplified reaction scheme (Eq. 1) to describe the change in composition of the apatite phase during maturation:



$\Delta G_{maturation}(i \rightarrow f)$  is given by  $\Delta G_{maturation}^\circ(i \rightarrow f) + RT \times \ln(K)$  where the equilibrium constant  $K$  is the activity product  $(\text{H}_2\text{PO}_4^-(aq))^{\delta_2} \times (\text{H}^+(aq))^{\delta_3}$  (which is close to the corresponding molar concentrations product for sufficiently dilute solutions where activity coefficients are close to 1). Taking as initial state the composition of the 20 min matured sample, and considering physiological conditions [pH = 7.4 and  $(\text{H}_2\text{PO}_4^-) \cong 10^{-4}$  M], this leads to negative values of  $\Delta G_{maturation}$  (at 298 K), ranging from 0 to  $-117 \pm 23$  kJ/mol. The value corresponding to evolution to stoichiometric HAP is  $-185 \pm 15$  kJ/mol. Although the effect of carbonation is not taken into account at this stage (thermodynamic data being not available yet for carbonated nanocrystalline apatites), and despite the simplified character of Equation 1, these calculations confirm that  $\text{H}_2\text{O}$  is essential and that maturation is strongly thermodynamically driven and give an order-of-magnitude estimate of the associated energetics.

The thermodynamic analysis suggests that immature apatite nanocrystals (e.g., as obtained right after bone remodeling) will inexorably evolve toward more mature compositions as long as they remain in humid conditions. This is not a trivial result as it underlines the fact that even before any “biological” consid-

erations, bone remodeling can be seen as dictated by physical chemistry (thermodynamics) where apatite nanocrystals, which have become too mature, stable, and less reactive, have to be dissolved (via osteoclast cells) and re-precipitated (via osteoblast cells) in a renewed immature state. Indeed, bone apatite plays an active role in homeostasis in vivo (Driessens et al. 1986), which requires that the high surface reactivity of the constituting nanocrystals (especially via their surface hydrated layer) allow surface ion exchanges to regulate plasma chemical composition, particularly of calcium and phosphate species.

### The impact of drying

Interruption of the maturation process can be achieved by separating the solid from the supernatant liquid, which will ultimately require some drying procedure. However, since water molecules are part of the crystal surface, drying is not a trivial task. The object of the present paper is not to examine and compare systematically various drying protocols; it aims, however, to stress the likely modification of the nanocrystal integrity upon such treatments. One way to inspect potential modifications is FTIR spectroscopy, as it is informative about the chemical environment of constitutive chemical species such as phosphates. Figure 7 reports the analysis of the  $\nu_3(\text{PO}_4)$  domain, and compares wet and dry states’ spectral features for a typical nanocrystalline apatite (matured a few minutes at 20 °C). A clear deformation of the spectrum can be evidenced upon (freeze)drying: although fine details can be observed on the freshly precipitated sample still wet (very close to the state of well-preserved bones, Grunewald et al. 2014), only a smoothed envelope of vibrational

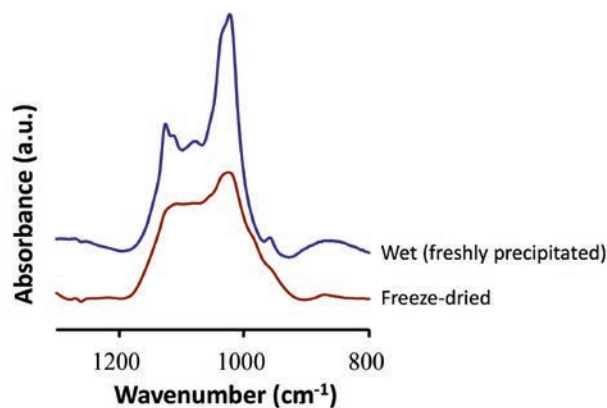


**FIGURE 7.** Effect of drying on the  $\nu_3(\text{PO}_4)$  domain as followed by FTIR spectroscopy for a nanocrystalline apatite sample matured few minutes at 20 °C. (Color online.)

features can be detected for the dried state. This effect suggests further disordering (seen in band broadening) of the surface layer, probably related to the loss of some water. Drying procedures are necessary for the preparation of most bone implants and care should be taken when selecting operating conditions as any (post)treatment of the nanocrystals may affect their integrity and should be examined in detail. This does not preclude the use of nanocrystalline apatite-based systems in medicine, as dried biomimetic apatites were shown to be biologically active and are the closest systems to natural bone. But one must stress that these compounds are hydrated and nanosized and thermodynamically metastable, and therefore they remain potentially sensitive to external treatments, e.g., for material processing, storage, or sterilization (Vandecastelaere et al. 2012).

From another angle, for the physical-chemical exploration of nanocrystalline apatites, drying/heating experiments can be envisioned to explore the progressive release of water, e.g., via TGA (see for example Yoder et al. 2012b). However, it may be remarked that the characteristic temperature of each contribution in thermal analyses is bound to depend upon the conditions of testing; faster heating leading to observation of peak maxima at higher temperature. In addition, importantly for carbonated samples,  $\text{HPO}_4^{2-}$  ions, if present, may interact with the carbonates during their thermal decomposition by reactions of the type:  $2 \text{HPO}_4^{2-} + \text{CO}_3^{2-} \rightarrow 2 \text{PO}_4^{3-} + \text{H}_2\text{O} + \text{CO}_2$  leading to significant lowering of the carbonate decomposition temperature, e.g., as low as 250 °C (Legros et al. 1982). Such interactions generate also superimposed effects, which increase the difficulty in accurately attributing weight losses to specific types of water in carbonated apatites.

### Type of associated water molecules

Even after (freeze)drying, apatite nanocrystals remain hydrated. Therefore a question arises as to the type of water molecules remaining in such nanocrystalline apatites. In the present contribution, to investigate this question, differential scanning calorimetry (DSC) measurements were performed, for the first time to our knowledge, on non-carbonated nanocrystalline apatites having undergone increasing maturation times. The samples were heated from −50 to 300 °C at 10 °C/min under a continuous flow of nitrogen. Figure 8a reports the typical heat flow signals obtained, with comparison to those of stoichiometric hydroxyapatite ( $\text{HAP}_{\text{st}}$ ). For all nanocrystalline apatite samples studied, clear endothermic peaks were seen (not taking into account the small artifact detected around 0 °C assignable to ice residue occurring systematically either on the reference or on the measurement compartment). More precisely, two main wide contributions were detected upon heating, with maxima observed at an average value of 63 °C (336 K) and 113 °C (386 K). In contrast, no such endotherm was detected for stoichiometric HAP (where only a slight endothermic contribution could be seen at higher temperatures, around 200 °C (473 K), due to the monoclinic → hexagonal phase transition, Suda et al. 1995). The occurrence of these peaks thus appears specific to immature nanocrystalline apatites. Note that TGA data also point to the loss of weight in this temperature range that can reasonably be attributed to water in these non-carbonated samples (Rollin-Martinet et al. 2013), and this weight loss was then used in the

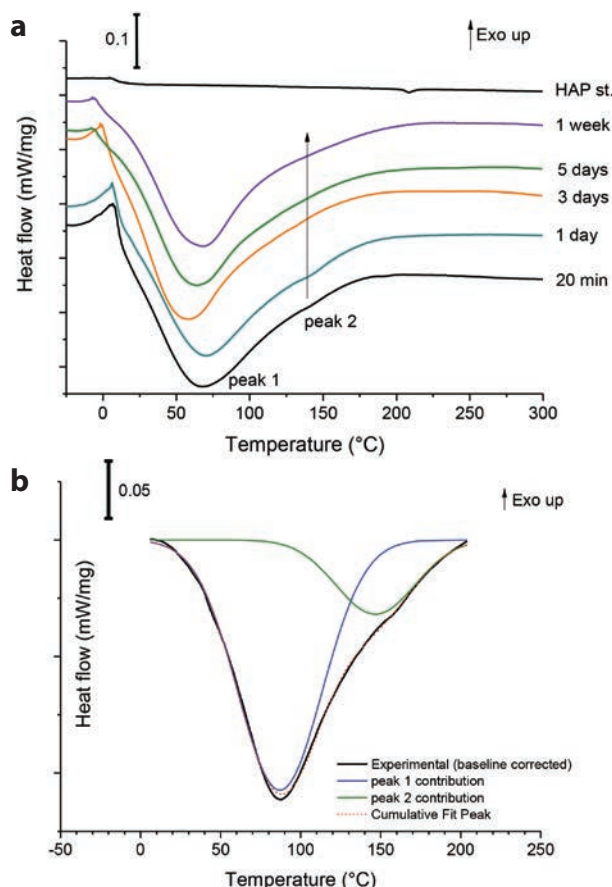


**FIGURE 8.** (a) DSC signal upon heating (at 10 °C/min) nanocrystalline apatites from 50 up to 300 °C under nitrogen flow, for various maturation times. Curves have been shifted intentionally for facilitating the reading. (b) Example of deconvolution of DSC signal for hap-1 day. (Color online.)

thermodynamic study to determine the total amount of water associated with the apatite compounds.

The endothermic contributions detected here may reasonably be attributed to the water constituting this hydrated interphase, plus the eventual water contained in the apatite structure itself (e.g., in apatite channels or in replacement of the oxygen vacancy left by the  $\text{CO}_3$ -for- $\text{PO}_4$  substitution), rather than to external/intercrystalline trapped water. Our observations of multiple peaks are similar to DSC data on lyophilized bovine bone, where three endothermic events were observed around 45, 91, and 126 °C (Galia et al. 2011). In that study, the authors tentatively attributed the peak at 45 °C to collagen denaturation and the peak at 91 °C to so-called “water associated with apatite,” while the peak at 126 °C was not discussed. Attribution of the 45 °C peak to collagen denaturation however appears questionable as this event generally occurs at higher temperature (Trębacz and Wójtowicz 2005). If the crystal/collagen interaction involves water, this peak may possibly be linked to alteration of this water at the interface. We believe that the peaks observed at 91 and 126 °C are related to the same origin (water loss) as in the present case on precipitated nanocrystalline apatites. Similarly, two endothermic overlapping events may be seen in the range 20–300 °C on DSC

curves reported by Capanema et al. (2015) on niobium-doped precipitated apatite; these events were attributed to “physically adsorbed water” but were not further discussed.

At this stage, it may be remarked that authors should be careful when referring to “adsorbed water” associated with apatite nanocrystals. Care should in particular be taken when dealing with water released well above 200 °C, which may hardly be assigned to simply “adsorbed,” as documented by Pasteris (2012). Furthermore, the terms “adsorbed water” are probably not the most appropriate to describe the water contained in the hydrated (and ionic) surface layer on apatite nanocrystals; indeed using this terminology may erroneously lead readers to consider it similar to the physisorbed water present on most solid surfaces exposed to moist, while H<sub>2</sub>O from the surface layer on apatite nanocrystals is instead closer from compositional water (even if it is not located in the apatitic core of the crystals). The terms “surface water” or “hydrated layer H<sub>2</sub>O” should probably be preferred.

Deconvolution of the DSC signals was carried out using the multiple peak fitting tool of the Origin 8.5 software and considering each (large) contribution as a Gaussian curve, thus allowing us to evaluate the relative proportion of each peak (see an example in Fig. 8b). Table 2 reports the results obtained. Considering the “low” temperature of the first endothermic peak, the associated water molecules released may be in a first approximation considered as energetically equivalent to liquid water, as is customary for loosely bound water. In this case, the energy  $\Delta H_1(\text{H}_2\text{O})$  required to eliminate one mole of water falls close to 42.5 kJ/mol allowing an estimate of the associated number of moles of water  $n_1(\text{H}_2\text{O}) = \Delta H_{\text{peak 1}} / \Delta H_1(\text{H}_2\text{O})$ . Subtracting this value from the total water content determined from TGA then allows evaluation of the number of moles of water associated with peak 2,  $n_2(\text{H}_2\text{O})$ . Finally, it is possible to estimate the energy needed to expel 1 mol of water in peak 2 (using the  $C_p$  of liquid water), giving  $\Delta H_2(\text{H}_2\text{O}) = 48.4 \pm 7.7$  kJ/mol at peak 2 temperature. This corresponds, at 25 °C (298 K), to  $52.1 \pm 7.7$  kJ/mol. This mean value is somewhat larger than the enthalpy of vaporization of water at 298 K (44 kJ/mol), suggesting that this H<sub>2</sub>O is indeed somewhat more strongly bound, but the difference is not beyond experimental error.

At least two contributions can thus be evidenced by DSC. The presence of water within the surface layer on the nanocrystals is undeniable as shown in the above and following sections and recently evidenced again by Wang et al. (2013) by solid-state NMR, and release from this surface water is thus expected upon heating. Some authors (e.g., Pasteris et al. 2014; Goldenberg et al. 2015), however, have concluded at least for carbonated systems

**TABLE 2.** DSC data for nanocrystalline apatites corresponding to increasing maturation times

Maturation time	$\Delta H_{\text{Total}}$ (kJ/mol)	$\Delta H_{\text{peak 1}}$ (kJ/mol)	$\Delta H_{\text{peak 2}}$ (kJ/mol)	$n_1(\text{H}_2\text{O})$ from peak 1 per mole of apatite	$n_2(\text{H}_2\text{O})$ from peak 2 per mole of apatite
20 min	176	88	88	2.1	1.8
3 h	178	110	68	2.6	1.4
1 day	143	72	72	1.7	1.5
3 days	169	90	78	2.1	1.6
5 days	147	70	76	1.7	1.6
1 week	137	80	57	1.9	1.2
3 weeks	143	95	47	2.3	1.0
1 day re-exposed	92	45	47	1.1	1.0

that a non-negligible amount of water molecules could fill apatite channels. At this stage, it is not possible to distinguish, from these DSC data, which portion of the associated water might be attributed to the surface layer H<sub>2</sub>O and which contribution may be related to intracrystalline water.

Upon maturation no clear trend could be identified for  $n_1(\text{H}_2\text{O})$ , reaching a mean around 2 mol H<sub>2</sub>O per unit formula (Fig. 9a). This may be linked, however, to the different “histories” of the freeze-dried samples in contact with the atmosphere for various periods of time. In contrast there is a progressive decrease of  $n_2(\text{H}_2\text{O})$ . The decrease in total water content observed is indeed expected, since the overall hydration of the nanocrystals is experimentally found to decrease with maturation.

To inspect the tendency for heated nanocrystalline apatites to partially rehydrate upon contact with moisture, a second DSC run was performed after one week of re-exposure to room atmosphere at ~20 °C on a sample (hap-1d) that already had undergone a DSC experiment up to 300 °C (Fig. 9b). Interestingly, the second run again shows the two clearly detectable peaks at essentially the same temperatures, although with lower intensities. These findings thus show that dehydrated apatite partially rehydrates upon simple re-exposure to water vapor. These observations further support dehydration/partial rehydration data reported by Yoder et al. (2012b). However it is remarkable to note that upon

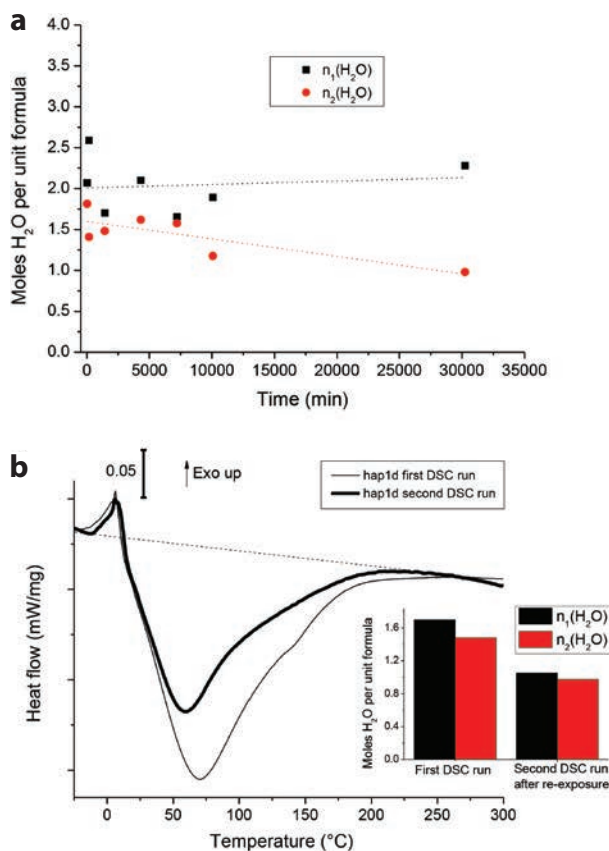


**FIGURE 9.** Evolution of  $n_1(\text{H}_2\text{O})$  and  $n_2(\text{H}_2\text{O})$  as evaluated from DSC data: (a) for samples with increasing maturation times and (b) effect of re-exposure to atmosphere on sample hap-1d. (Color online.)



such rehydration, both DSC peaks are affected, indicating that the water related to these two peaks is at least partly reversibly released, which in turn suggests partial “water refilling” of (at least) the surface layer.

These results again point out the key role of water that systematically “associates with” apatite nanocrystals when they are exposed to a wet environment. The question, however, still remains as to whether intracrystalline water is also present or not in all nanocrystalline apatite samples. For carbonated apatites, several authors agreed on the presence of water in the apatitic lattice, like Ivanova et al. (2001) on the basis of Rietveld refinements of XRD data, or else LeGeros et al. (1978, 1979), Bonel et al. (1975), and Labarthe et al. (1973) on the basis of thermal analyses sometimes assisted by IR analyses, and as reviewed by Pasteris et al. (2014). However, whether this conclusion may be widened to all nanocrystalline apatites including non-carbonated ones is still unclear. There is a lack of direct correlation between the amount of such intracrystalline water and the number of OH vacancies (Pasteris et al. 2014); the amount of H<sub>2</sub>O remaining essentially unchanged for all of samples tested in that work. These findings are reminiscent of those obtained in an earlier work by LeGeros et al. (1979) but appear surprising as water molecules, if incorporated in the apatitic channels, would be expected to fill these positions more easily in the case of more OH-deficient samples. However, other parameters such as the co-presence of Na<sup>+</sup> ions might also come into play, although no clear mechanism can yet be formulated precisely. Indeed, the two studies cited above involved sodium ions, while experiments performed in sodium-free conditions led to different results, pointing then to a correlation between the level of carbonation and the total associated water (Labarthe et al. 1973). Also, intracrystalline water might otherwise be located, in carbonated samples, in other positions than apatitic channels, as in the oxygen vacancy left by the substitution of a phosphate by a B-type carbonate group or in calcium vacancies (e.g., Bonel et al. 1975; Ivanova et al. 2001); and water location may even depend on formation conditions. Compositional differences that affect the size of the apatite channels may also affect the amount of intracrystalline water (Goldenberg et al. 2015). In the present DSC study on non-carbonated samples, the re-observation of the two DSC peaks by simple exposure to ambient air seems to favor the hypothesis of surface water refilling rather than a more internal phenomenon, but additional investigations on various types of nanocrystalline apatite are needed to continue to explore the different locations/types of water molecules, depending on their conditions of formation.

### **Role of surface water on the spatial organization of apatite nanocrystals**

It is interesting at this stage to inspect the role of surface water molecules in the 3D organization of the nanocrystals in a situation where alteration due to drying has been limited as far as possible. In a specific set of experiments, freshly precipitated apatite nanocrystals were left to mature at 25 °C in the mother solution between 1 min and 1 week, prior to sampling the precipitating medium and analyzing it immediately by cryo-FEG-SEM; the cryogenic mode was selected to limit insofar as possible any alteration of the samples. Figure 10 shows the

typical morphologies obtained. A clear evolution is seen in the course of maturation in solution. At  $t = 1$  min, the precipitate appears as a three-dimensional network of spheroid-like particles with a mean diameter around 15 nm, these spheroids tending to organize themselves in pseudo-filaments or relatively linear chains. Progressively, the spheroids evolve toward a more acicular morphology, typically over the first 12 h. At  $t = 12$  h, they have almost totally transformed into a three-dimensional arrangement of elongated particles, with a mean length around 50–70 nm and a width close to 10 nm. From then on, the elongated particles are clearly visible and seem to organize in a parallel fashion as “bundles” linked by an amorphous-like domain. At  $t = 1$  week, the particles reach a mean length of about 100 nm and a width of about 7–8 nm and the bundles are still clearly visible. A schematic representation of these morphological modifications is given on Figure 10 (bottom). It may be noted that the mean size of the spheroids (at  $t = 1$  min) is of the same order as the crystallite dimensions estimated from XRD data and Scherrer’s formula (see Fig. 4c), suggesting that these spheroids could be individual crystallites. In contrast, for longer maturation times, the elongated particles exhibit dimensions close to 100 nm, which is significantly larger than individual crystallites. We can then assume the formation of polycrystalline particles involving crystallites in strong interaction with each other (aggregation). We have studied the effect of dilution of the precipitation medium on the general aspect of the precipitate, and similar conclusions have been drawn; in particular, bundles of particles were still present but in the form of more separated “islands” dispersed in water. Within each bundle, an amorphous-like domain was still noticed. It may be suggested that the interaction of adjacent nanocrystals via their surface hydrated layers plays a major role in this 3D organization of apatite particles, in particular their tendency to orient in parallel to form bundle-like superstructures. This 3D organization seems to be characteristic of apatite nanocrystals as this has never been reported to our knowledge for well-crystallized hydroxyapatite (which does not exhibit a hydrated layer on its constitutive crystals). This difference may be due to the elongated or flattened morphology of the particles, favoring alignment between most-developed crystal surfaces; but the involvement of the hydrated domains on the nanocrystals, capable of interacting with each other, also appears as a probable hypothesis. The exact mechanism by which adjacent nanocrystals, by way of their hydrated layers, can interact is still unclear. It may involve electrostatic interaction and/or hydrogen bonding between water molecules or HPO<sub>4</sub><sup>2-</sup> ions; the high mobility of ions within this layer may also help interlacing between two adjacent layers by facilitating diffusive pathways. It may be assumed that a similar scenario of apatite particle alignment should also appear in bone in vivo. Wang et al. (2013) have indeed noticed a similar tendency for bone crystals to orient in parallel, which is in good agreement with our data on synthetic biomimetic analogs. Such alignment, particularly in a favored direction, may be important in bone repair processes. Indeed, the callus tissue formed upon fracture healing also was found to exhibit preferential crystal orientations (Liu et al. 2010). From another perspective, low-gravity environments in space have been shown to accelerate bone loss. Although bone cell activity was shown to be altered under microgravity (Nabavi et al. 2011), the underlying mecha-

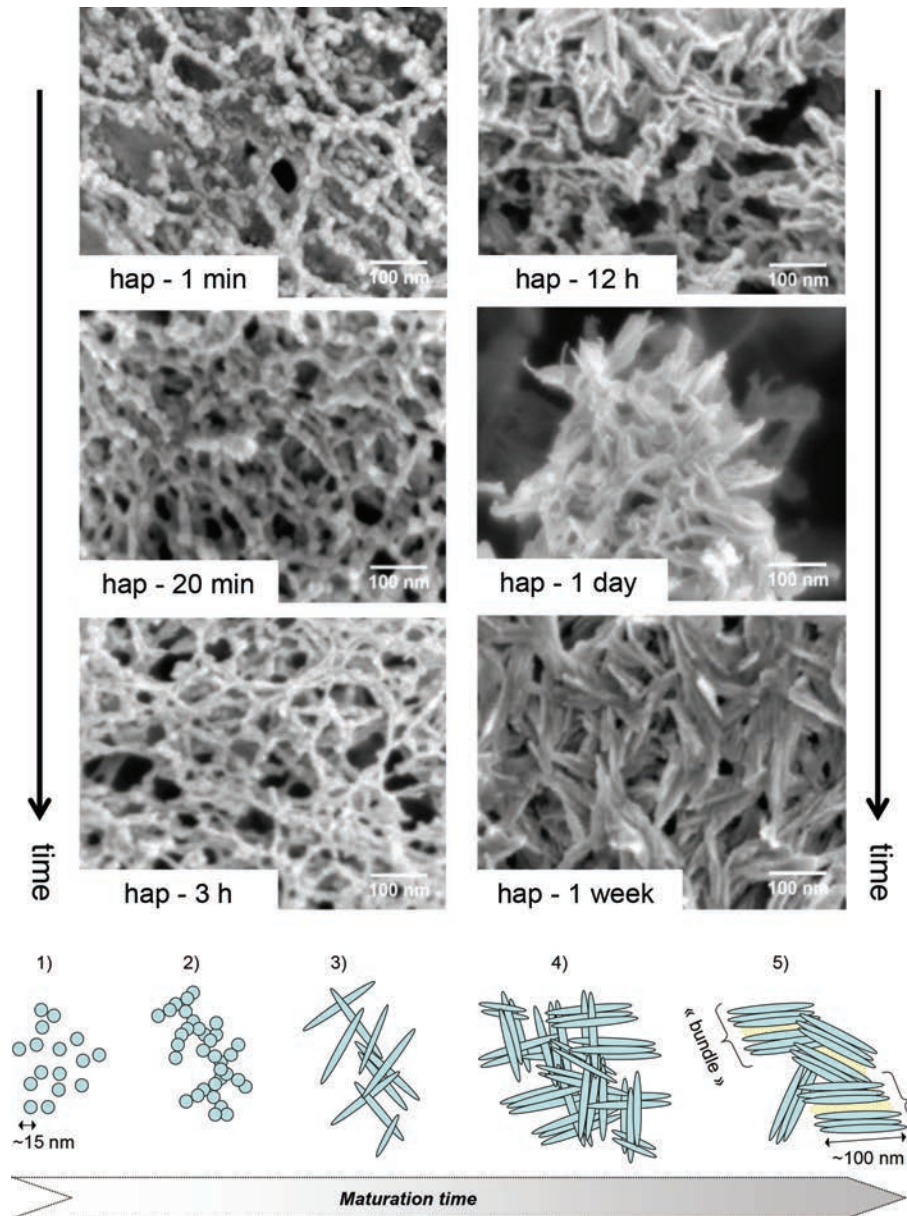


**FIGURE 10.** Cryo-FEG-SEM observations of nanocrystalline apatites matured at 25 °C between 1 min and 1 week and directly analyzed (initial magnification: 150 000 $\times$ ), and schematic representation of the evolutionary change of morphology. (Color online.)

nism is unclear; whether crystal alignment may be influential in the response of bone to microgravity is still unknown.

### Consolidation behavior

These findings point out the strong tendency for apatite nanocrystals to interact with each other via their hydrated surface layers. It is thus interesting to investigate the possibility to consolidate these systems into bulk ceramics utilizing this propensity for self-organization. This has been done by way of spark plasma sintering (SPS) at "low" temperature, typically below 300 °C. The first trials of such "cold sintering" having been performed in 2006 (Drouet et al. 2006) and revisited later

in detail by Grossin et al. (2010) for hap-1d. Consolidation of nanocrystalline apatite by SPS was shown to be effective. Sintering for 13 min at 150 °C under 100 MPa was found to be the best compromise between a high densification rate and a limitation of nanocrystals alteration. Bulk ceramic pieces were obtained with mechanical properties allowing applications for bone repair. For example, the flexural strength measured from 7 samples of hap-1d by biaxial flexural tests reached  $11.3 \pm 5.9$  MPa. This value is high for a material sintered at 150 °C (the non-negligible standard deviation probably results from the defects present in the raw material consolidated by SPS). In contrast, SPS treatment beyond 150 °C led to a delamination phenomenon. We can pro-

pose that (1) the consolidation process at such low temperatures is made possible by the presence of interacting surface layers on adjacent nanocrystals allowing easier ion diffusion, and that (2) the delamination observed at “higher” temperatures is linked to significant dehydration of apatite nanocrystals, altering the surface layer and preventing efficient ion diffusion. This ability for apatite nanocrystals to consolidate appears to be a very peculiar property of these compounds as they remain noticeably hydrated. This conclusion is also supported in the present work by the consolidation of nanocrystalline apatites having different maturation times, using the same SPS protocol as above (13 min at 150 °C, 100 MPa). However, the relative density of the ceramics noticeably decreased for samples of increasing maturation times (typically from 77% for hap-20 min down to 53% for hap-3 weeks). In addition to the small size of the crystals favoring re-orientation under mechanical pressure, the extent of the hydrated layer appears to have a direct effect on their sinterability. The consolidation/sintering of nanocrystalline apatites at “low” temperature may be made possible thanks to the high mobility of ions contained in the hydrated layer. To check surface ion mobility, rapid (few minutes) ion exchange experiments were carried out as previously (Drouet et al. 2008; Eichert et al. 2007). Here, we immersed nanocrystalline apatites in a solution containing  $Mg^{2+}$  ions at high concentration (1 M) for 30 min, and followed the replacement of (surface)  $Ca^{2+}$  ions by  $Mg^{2+}$  by ICP-AES by analyzing the solids before and after ion exchange. Figure 11 reports the results obtained in terms of “exchangeable” and “non-exchangeable”  $Ca^{2+}$  ions. These data show that samples matured for short periods of time exhibit a noticeable amount of exchangeable ions (e.g., up to 8% of the total  $Ca^{2+}$  content), while this amount decreases with maturation time. These results illustrate the high mobility of surface ions from nanocrystalline apatites. In the context of consolidation, as in SPS, this high mobility could allow diffusion phenomena even at “low/moderate” temperatures, while not necessitating strong thermal activation, thus allowing cold sintering. A partial loss of water also appears essential for the consolidation (Grossin et al. 2010), as it allows strong interaction between adjacent crystals.

### Extrapolation to the in vivo context

Although most of the data given above concern non-carbonated apatites, it is very likely that similar general conclusions can be made for their carbonated counterparts. Indeed, carbonate ions are known as growth inhibitors for apatite (Sallis 1998); a carbonated apatite exhibits a more developed hydrated surface layer than its non-carbonated counterpart for the same aging time in solution. In vivo, the ion exchange capabilities of apatite nanocrystals represent a way for bone mineral to be active in homeostasis. The natural ability of apatite nanocrystals to align in a parallel way when in wet conditions is likely to occur also in vivo, and results from Wang et al. (2013) corroborate this assumption. Like their biomimetic analogs, bone nanocrystals are expected to be thermodynamically metastable, leading to unavoidable evolution toward more stable compositions, closer to stoichiometry. This is probably one non-biological reason for the necessity of bone remodeling, where more mature crystals (becoming less surface-reactive) are progressively dissolved and replaced by new immature, highly reactive nanocrystals.

## IMPLICATIONS

All of the above has illustrated the key role of water in the genesis, evolution in solution, 3D particle organization, and general behavior (e.g., via consolidation) of nanocrystalline apatites, whether in bone or in synthetic analogs. The presence of water associated with apatite nanocrystals should therefore not be overlooked, but instead  $H_2O$  should be considered as a component of the crystal’s composition, at least on its surface. Its elimination, e.g., via drying/heating processes, may fundamentally modify the crystals surface features and reactivity. The surface layer covering the nanocrystals appears as an interphase with potentially gradual properties linking the crystals to the surrounding medium. This hydrated interphase might be seen as a remnant of the apatite growth process in solution. Whether it involves, in early stages, the formation of prenucleation clusters is still undetermined. In any case the apatite and its hydrated layer should be considered, in our opinion, as appearing simultaneously. Intermediate metastable phases, e.g., amorphous calcium phosphate or “ACP,” may transiently be formed in the precipitating medium, depending on the apatite formation conditions. ACP is likely involved for example in the preparation of synthetic analogs where concentrations/supersaturation are generally higher than in vivo; and apatite may then crystallize from the amorphous phase. A question can then arise as whether the formation and evolution/growth of apatite nuclei within this ACP might structure the crystal and its surface layer, but this is still under study. Another phenomenon should also be considered when dealing with the formation of apatite from an amorphous phase without changing the Ca/P ratio: the internal hydrolysis of  $PO_4^{3-}$  ions. In this process, the simultaneous formation of  $OH^-$  and  $HPO_4^{2-}$  ions arises from reaction of water with  $PO_4^{3-}$  ions. It is not clear however whether this reaction occurs in bone or not. IR and Raman spectroscopies only point to limited amounts of  $OH^-$  even for mature bone (e.g., Pasteris et al. 2004; Rey et al. 1995). NMR seems in contrast to identify larger hydroxide

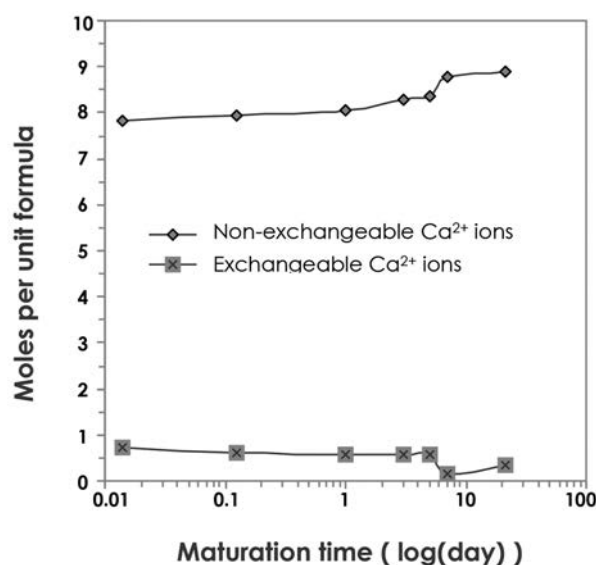


FIGURE 11. Evolution of exchangeable  $Ca^{2+}$  ions by  $Mg^{2+}$  by surface ion exchanges for apatites with increasing maturation times



contents (e.g., Cho et al. 2003), but this internal hydrolysis reaction might explain the relative divergence between vibrational spectroscopies and NMR, taking into account the fact that NMR generates some sample heating and necessitates longer acquisition times than Raman or IR.

The location of water molecules in bone apatite nanocrystals and biomimetic analogs is still being debated and explored. The presence of water within the surface layer on the nanocrystals is obvious, but additional water is also reported for carbonated apatites to be trapped in the structure although incorporation mechanisms have still to be clarified. As a perspective, additional exploration of the water environments within the surface layer and inside the structure is needed to better comprehend biomineralization phenomena as well as biomimetic apatite-based biomaterials processing. In addition, methods should be further developed for quantifying the relative volume of the hydrated layer covering apatite nanocrystals, and the relative amounts of water in the various reservoirs associated with nanocrystalline apatites.

## ACKNOWLEDGMENTS

The authors thank the Agence Nationale de la Recherche (ANR) for funding in the scope of the NanoBioCer and BioCapabili projects (ANR-07-BLAN-0373 and PICF 2009). The thermodynamic work at Davis was supported by the France Berkeley Fund (FBF) and the Institut National Polytechnique de Toulouse (INPT). The authors also thank the GdR CNRS no. 3584 TherMatHT ([www.thermatht.fr](http://www.thermatht.fr)) and the Thermodynamics Consortium ([www.thermocon.org](http://www.thermocon.org)) for fruitful discussion and collaborative work on the present contribution.

## REFERENCES CITED

- Bonel, G., Labarthe, J.C., and Vignoles, C. (1975) Contribution à l'étude structurale des apatites carbonatées de type B. In CNRS, Ed., *Physico-Chimie et Cristallographie des Apatites d'intérêt Biologique*, p. 117–125. Colloques Internationaux du Centre National de la Recherche Scientifique, Paris.
- Bonjour, J.P. (2011) Calcium and phosphate: A duet of ions playing for bone health. *Journal of the American College of Nutrition*, 30, 438S–448S.
- Bouladjine, A., Al-Kattan, A., Dufour, P., and Drouet, C. (2009) New advances in nanocrystalline apatite colloids intended for cellular drug delivery. *Langmuir*, 25, 12256–12265.
- Capanema, N.S.V., Mansur, A.A.P., Carvalho, S.M., Silva, A.R.P., Ciminelli, V.S., and Mansur, H.S. (2015) Niobium-doped hydroxyapatite bioceramics: Synthesis, characterization and in vitro cytocompatibility. *Materials*, 8, 4191–4209.
- Carlström, D., Glas, J.E., and Angmar, B. (1963) Studies on the ultrastructure of dental enamel: V. The state of water in human enamel. *Journal of Ultrastructure Research*, 8, 24–29.
- Cazalbou, S., Combes, C., Eichert, D., Rey, C., and Glimcher, M.J. (2004a) Poorly crystalline apatites: evolution and maturation in vitro and in vivo. *Journal of Bone and Mineral Metabolism*, 22, 310–317.
- Cazalbou, S., Eichert, D., Drouet, C., Combes, C., and Rey, C. (2004b) Biological mineralisations based on calcium phosphate. *Comptes Rendus Palevol*, 3, 563–572.
- Chander, S., and Fuerstenau, D.W. (1984) Solubility and interfacial properties of hydroxyapatite: a review. In D.N. Misra, Ed., *Adsorption on and Surface Chemistry of Hydroxyapatite*, p. 29–49. Plenum Press, New York.
- Cho, G., Wu, Y., and Ackerman, J.L. (2003) Detection of hydroxyl ions in bone mineral by solid-state NMR spectroscopy. *Science*, 300, 1123–1127.
- Chowdhury, E.H., and Akaïke, T. (2005) Advances in fabrication of calcium phosphate nano-composites for smart delivery of DNA and RNA to mammalian cells. *Current Analytical Chemistry*, 1, 187–192.
- Delgado-Lopez, J.M., Iafisco, M., Rodriguez, I., Tampieri, A., Prat, M., and Gomez-Morales, J. (2012) Crystallization of bioinspired citrate-functionalized nanoapatite with tailored carbonate content. *Acta Biomaterialia*, 8, 3491–3499.
- Della Gatta, G., Richardson, M.J., Sarge, S.M., and Stølen, S. (2006) Standards, calibration, and guidelines in microcalorimetry. Part 2. Calibration standards for differential scanning calorimetry (IUPAC Technical Report). *Pure and Applied Chemistry*, 78, 1455.
- Driessens, F.C.M., Vandijk, J.W.E., and Verbeeck, R.M.H. (1986) The role of bone-mineral in calcium and phosphate homeostasis. *Bulletin Des Societes Chimiques Belges*, 95, 337–342.
- Drouet, C. (2013) Apatite formation: Why it may not work as planned, and how to conclusively identify apatite compounds. *BioMed Research International* 2013, Article ID 490946, 1–12.
- Drouet, C., Largeot, C., Raimbeaux, G., Estournes, C., Dechambre, G., Combes, C., and Rey, C. (2006) Bioceramics: spark plasma sintering (SPS) of calcium phosphates. *Advances in Science and Technology*, 49, 45–50.
- Drouet, C., Carayon, M.-T., Combes, C., and Rey, C. (2008) Surface enrichment of biomimetic apatites with biologically-active ions  $Mg^{2+}$  and  $Sr^{2+}$ : A preamble to the activation of bone repair materials. *Materials Science and Engineering C*, 28, 1544–1550.
- Drouet, C., Bosc, F., Banu, M., Largeot, C., Combes, C., Dechambre, G., Estournes, C., Raimbeaux, G., and Rey, C. (2009) Nanocrystalline apatites: From powders to biomaterials. *Powder Technology*, 190, 118–122.
- Drouet, C., Al-Kattan, A., Choimet, M., Tourrette, A., Santran, V., Dexpert-Ghys, J., Pipy, B., Brouillet, F., and Tourbin, M. (2015) Biomimetic apatite-based functional nanoparticles as promising newcomers in nanomedicine: Overview of 10 years of initiatory research. *Journal of General Practice and Medical Diagnosis (GPMDD)*, 1, 1–9.
- Eichert, D. (2001) Etude de la reactivite de surface d'apatites de synthese nanocrystallines. Ph.D. thesis, Institut National Polytechnique de Toulouse, France.
- Eichert, D., Combes, C., Drouet, C., and Rey, C. (2005) Formation and evolution of hydrated surface layers of apatites. *Key Engineering Materials*, 284–286, 3–6.
- Eichert, D., Drouet, C., Sifhi, H., Rey, C., and Combes, C. (2007) Nanocrystalline apatite based biomaterials: synthesis, processing and characterization. In J.B. Kendall, Ed., *Biomaterials Research Advances*, p. 93–143. Nova Science Publishers, New York.
- Elliott, J.C. (1994) *Structure and Chemistry of the Apatites and Other Calcium Orthophosphates*, 389 p. Elsevier, Amsterdam.
- Galia, C.R., Lourenço, A.L., Rosito, R., Macedo, C.A.S., and Camargo, L.M.A.Q. (2011) Caracterização físico-química do enxerto de osso bovino liofilizado. *Revista Brasileira de Ortopedia*, 46, 444–451.
- Glimcher, M.J. (1959) Molecular biology of mineralized tissues with particular reference to bone. *Reviews of Modern Physics*, 31, 359–393.
- Goldenberg, J.E., Wilt, Z., Schermerhorn, D.V., Pasteris, J.D., and Yoder, C.H. (2015) Structural effects on incorporated water in carbonated apatites. *American Mineralogist*, 100, 274–280.
- Gomez-Morales, J., Iafisco, M., Delgado-Lopez, J.M., Sarda, S., and Drouet, C. (2013) Progress on the preparation of nanocrystalline apatites and surface characterization: Overview of fundamental and applied aspects. *Progress in Crystal Growth and Characterization of Materials*, 59, 1–46.
- Grahame, D.C. (1947) The electrical double layer and the theory of electrocapillarity. *Chemical Reviews*, 41, 441–501.
- Granke, M., Does, M.D., and Nyman, J.S. (2015) The role of water compartments in the material properties of cortical bone. *Calcified Tissue International*, 97, 292–307.
- Grossin, D., Rollin-Martin, S., Estournes, C., Rossignol, F., Champion, E., Combes, C., Rey, C., Chevallier, G., and Drouet, C. (2010) Biomimetic apatite sintered at very low temperature by spark plasma sintering: Physico-chemistry and microstructure aspects. *Acta Biomaterialia*, 6, 577–585.
- Grunenwald, A., Keyser, C., Sautereau, A.M., Crubezy, E., Ludes, B., and Drouet, C. (2014) Novel contribution on the diagenetic physicochemical features of bone and teeth minerals, as substrates for ancient DNA typing. *Analytical and Bioanalytical Chemistry*, 406, 4691–4704.
- Grynaps, M. (1976) Crystallinity of bone-mineral. *Journal of Materials Science*, 11, 1691–1696.
- Habraken, W.J., Tao, J., Brylka, L.J., Friedrich, H., Bertinetti, L., Schenk, A.S., Verch, A., Dmitrovic, V., Bomans, P.H., Frederik, P.M., and others. (2013) Ion-association complexes unite classical and non-classical theories for the biomimetic nucleation of calcium phosphate. *Nature Communications*, 4, 1507, 1–12.
- Hossain, S., Stanislaus, A., Chua, M.J., Tada, S., Tagawa, Y.-i., Chowdhury, E.H., and Akaïke, T. (2010) Carbonate apatite-facilitated intracellularly delivered siRNA for efficient knockdown of functional genes. *Journal of Controlled Release*, 147, 101–108.
- Iafisco, M., Delgado-Lopez, J.M., Gomez-Morales, J., Hernandez-Hernandez, M.A., Rodriguez-Ruiz, I., and Roveri, N. (2011) Formation of calcium phosphates by vapour diffusion in highly concentrated ionic micro-droplets. *Crystal Research and Technology*, 46, 841–846.
- Iafisco, M., Palazzo, B., Martra, G., Margiotta, N., Piccinonna, S., Natile, G., Gandin, V., Marzano, C., and Roveri, N. (2012) Nanocrystalline carbonate-apatites: role of Ca/P ratio on the upload and release of anticancer platinum bisphosphonates. *Nanoscale*, 4, 206–217.
- Iafisco, M., Manuel Delgado-Lopez, J., Varoni, E.M., Tampieri, A., Rimondini, L., Gomez-Morales, J., and Prat, M. (2013) Cell surface receptor targeted biomimetic apatite nanocrystals for cancer therapy. *Small*, 9, 3834–3844.
- Ivanova, T.I., Frank-Kamenetskaya, O.V., Kol'tsov, A.B., and Ugolkov, V.L. (2001) Crystal structure of calcium-deficient carbonated hydroxyapatite. Thermal decomposition. *Journal of Solid State Chemistry*, 160, 340–349.
- Jäger, C., Welzel, T., Meyer-Zaika, W., and Epple, M. (2006) A solid-state NMR investigation of the structure of nanocrystalline hydroxyapatite. *Magnetic Resonance in Chemistry*, 44, 573–580.
- Kaflak, A., and Kolodziejewski, W. (2008) Kinetics H-1 → P-31 NMR cross-polarization in bone apatite and its mineral standards. *Magnetic Resonance in Chemistry*, 46, 335–341.
- Kramer, E., Itzkowitz, E., and Wei, M. (2014) Synthesis and characterization of cobalt-substituted hydroxyapatite powders. *Ceramics International*, 40, 13471–13480.
- Labarthe, J.C., Bonel, G., and Montel, G. (1973) Sur la structure et les propriétés des apatites carbonatées de type B phosphocalciques. *Annales de Chimie*, 8, 289–301.

- LeGeros, R.Z., and LeGeros, J.P. (1984) Phosphate minerals in human tissues. In J.O. Nriagu and P.B. Moore, Eds., *Phosphate Minerals*, p. 351–385. Springer.
- LeGeros, R.Z., Bonel, G., and Legros, R. (1978) Types of  $H_2O$  in human enamel and in precipitated apatites. *Calcified Tissue Research*, 26, 111–118.
- LeGeros, R.Z., Legros, R., and Bonel, G. (1979) Sur la déshydratation des apatites carbonatées de type B sodées. *Compte-Rendu de l'Académie des Sciences-Paris*, 288 C, 81–84.
- Legros, R., Godinot, C., Torres, L., Mathieu, J., and Bonel, G. (1982) Sur la stabilité thermique des carbonates du tissu osseux. *Journal de Biologie Buccale*, 10, 3–9.
- Legros R., Balmain N., and Bonel G. (1987) Age-related changes in mineral of rat and bovine cortical bone. *Calcified Tissue Research*, 41, 137–144.
- Liu, Y., Manjubala, I., Roschger, P., Schell, H., Duda, G.N., and Fratzl, P. (2010) Mineral crystal alignment in mineralized fracture callus determined by 3D small-angle X-ray scattering. *Journal of Physics: Conference Series*, 247, 012031.
- Lu, H.B., Campbell, C.T., Graham, D.J., and Ratner, B.D. (2000) Surface characterization of hydroxyapatite and related calcium phosphates by XPS and TOF-SIMS. *Analytical Chemistry*, 72, 2886–2894.
- Luong, H.V.T., and Liu, J.C. (2017) Flotation separation of strontium via phosphate precipitation. *Water Science and Technology*, 75, 2520–2526.
- Mancardi, G., Terranova, U., and de Leeuw, N.H. (2016) Calcium phosphate prenucleation complexes in water by means of ab initio molecular dynamics simulations. *Crystal Growth & Design*, 16, 3353–3358.
- Nabavi, N., Khandani, A., Camirand, A., and Harrison, R.E. (2011) Effects of microgravity on osteoclast bone resorption and osteoblast cytoskeletal organization and adhesion. *Bone*, 49, 965–74.
- Neuman, W.F., and Neuman, M.W. (1953) The nature of the mineral phase of bone. *Chemical Reviews*, 53, 1–45.
- Neuman, W.F., Toribara, T.Y., and Mulryan, B.J. (1953) The surface chemistry of bone. VII. The Hydration Shell. *Journal of the American Chemical Society*, 75, 4239–4242.
- Nyman, J.S., Roy, A., Shen, X., Acuna, R.L., Tyler, J.H., and Wang, X. (2006) The influence of water removal on the strength and toughness of cortical bone. *Journal of Biomechanics*, 39, 931–938.
- Nyman, J.S., Ni, Q., Nicoletta, D.P., and Wang, X. (2008) Measurements of mobile and bound water by nuclear magnetic resonance correlate with mechanical properties of bone. *Bone*, 42, 193–9.
- Pasteris, J.D. (2012) Structurally incorporated water in bone apatite: A cautionary tale. In R.B. Heimann, Ed., *Calcium Phosphates: Structure, Synthesis, Properties, and Applications*, p. 63–94. Nova Science Publishers, New York.
- Pasteris, J.D., Wopenka, B., Freeman, J.J., Rogers, K., Valsami-Jones, E., van der Houwen, J.A.M., and Silva, M.J. (2004) Lack of OH in nanocrystalline apatite as a function of degree of atomic order: implications for bone and biomaterials. *Biomaterials*, 25, 229–238.
- Pasteris, J.D., Yoder, C.H., Sterlieb, M.P., and Liu, S. (2012) Effect of carbonate incorporation on the hydroxyl content of hydroxylapatite. *Mineralogical Magazine*, 76, 2741–2759.
- Pasteris, J.D., Yoder, C.H., and Wopenka, B. (2014) Molecular water in nominally unhydrated carbonated hydroxylapatite: The key to a better understanding of bone mineral. *American Mineralogist*, 99, 16–27.
- Raynaud, S., Champion, E., Bernache-Assollant, D., and Thomas, P. (2002) Calcium phosphate apatites with variable Ca/P atomic ratio I. Synthesis, characterisation and thermal stability of powders. *Biomaterials*, 23, 1065–1072.
- Rey, C., Lian, J., Grynias, M., Shapiro, F., Zylberberg, L., and Glimcher, M.J. (1989) Non-apatitic environments in bone mineral: FT-IR detection, biological properties and changes in several disease states. *Connective Tissue Research*, 21, 267–73.
- Rey, C., Shimizu, M., Collins, B., and Glimcher, M.J. (1990) Resolution-enhanced Fourier-transform infrared-spectroscopy study of the environment of phosphate ions in the early deposits of a solid-phase of calcium-phosphate in bone and enamel, and their evolution with age. I. Investigations in the  $\nu_1PO_4$  domain. *Calcified Tissue International*, 46, 384–394.
- Rey, C., Miquel, J.L., Facchini, L., Legrand, A.P., and Glimcher, M.J. (1995) Hydroxyl groups in bone mineral. *Bone*, 16, 583–586.
- Rey, C., Combes, C., Drouet, C., Sfihi, H., and Barroug, A. (2007) Physico-chemical properties of nanocrystalline apatites: Implications for biominerals and biomaterials. *Materials Science and Engineering C*, 27, 198–205.
- Rey, C., Combes, C., Drouet, C., and Glimcher, M. (2009) Bone mineral: update on chemical composition and structure. *Osteoporosis International*, 20, 1013–1021.
- Rey, C., Combes, C., Drouet, C., Cazalbou, S., Grossin, D., Brouillet, F., and Sarda, S. (2014a) Surface properties of biomimetic nanocrystalline apatites; applications in biomaterials. *Progress in Crystal Growth and Characterization of Materials*, 60, 63–73.
- Rey, C., Marsan, O., Combes, C., Drouet, C., Grossin, D., and Sarda, S. (2014b) Characterization of calcium phosphates using vibrational spectroscopies. In B. Ben-Nissan, Ed., *Advances in Calcium Phosphate Biomaterials*, 2, p. 229–266. Springer.
- Robie, R.A., and Hemingway, B.S. (1995) Thermodynamic properties of minerals and related substances at 298.15 K and 1 bar ( $10^5$  pascals) pressure and at higher temperatures. U.S. Geological Survey Bulletin, 2131.
- Rollin-Martinet, S. (2011) Développement de nouvelles bioceramiques par consolidation à basse température d'apatites nanocrystallines biomimétiques. Ph.D. thesis, Université de Limoges, France.
- Rollin-Martinet, S., Navrotsky, A., Champion, E., Grossin, D., and Drouet, C. (2013) Thermodynamic basis for evolution of apatite in calcified tissues. *American Mineralogist*, 98, 2037–2045.
- Roufousse, A.H., Aue, W.P., Roberts, J.E., Glimcher, M.J., and Griffin, R.G. (1984) Investigation of the mineral phases of bone by solid-state P-31 magic angle sample spinning nuclear magnetic-resonance. *Biochemistry*, 23, 6115–6120.
- Sallis, J.D. (1998) Structure/performance relationships of phosphorous and carboxyl containing additives as calcium phosphate crystal growth inhibitors. In Z. Amjad, Ed., *Calcium Phosphates in Biological and Industrial Systems*, p. 173–191. Kluwer Academic, Dordrecht.
- Sfihi, H., and Rey, C. (2002) 1-D and 2-D double heteronuclear magnetic resonance study of the local structure of Type B carbonate fluoroapatite. In J. Fraissard and O. Lapina, Eds., *Magnetic Resonance in Colloid and Interface Science*, p. 409–422. Springer.
- Sokolova, V.V., Radtke, I., Heumann, R., and Eppler, M. (2006) Effective transfection of cells with multi-shell calcium phosphate-DNA nanoparticles. *Biomaterials*, 27, 3147–3153.
- Stefanic, M., Ward, K., Tawfik, H., Seemann, R., Baulin, V., Guo, Y., Fleury, J.-B., and Drouet, C. (2017) Apatite nanoparticles strongly improve red blood cell cryopreservation by mediating trehalose delivery via enhanced membrane permeation. *Biomaterials*, 140, 138–149.
- Suda, H., Yashima, M., Kakihana, M., and Yoshimura, M. (1995) Monoclinic  $\leftrightarrow$  hexagonal phase transition in hydroxyapatite studied by X-ray powder diffraction and differential scanning calorimeter techniques. *The Journal of Physical Chemistry*, 99, 6752–6754.
- Timmins, P.A., and Wall, J.C. (1977) Bone water. *Calcified Tissue Research*, 23, 1–5.
- Trębacz, H., and Wójtowicz, K. (2005) Thermal stabilization of collagen molecules in bone tissue. *International Journal of Biological Macromolecules*, 37, 257–262.
- Unal, M., and Akkus, O. (2015) Raman spectral classification of mineral- and collagen-bound water's associations to elastic and post-yield mechanical properties of cortical bone. *Bone*, 81, 315–26.
- Ushakov, S.V., Helean, K.B., Navrotsky, A., and Boatner, L.A. (2001) Thermochemistry of rare-earth orthophosphates. *Journal of Materials Research*, 16, 2623–2633.
- Vandecastelaere, N., Rey, C., and Drouet, C. (2012) Biomimetic apatite-based biomaterials: on the critical impact of synthesis and post-synthesis parameters. *Journal of Materials Science-Materials in Medicine*, 23, 2593–2606.
- Wagman, D.D., Evans, W.H., Parker, V.B., Schumm, R.H., Halow, I., Bailey, S.M., Churney, K.L., and Nuttall, R.L. (1982) The NBS tables of chemical thermodynamic properties—Selected values for inorganic and C-1 and C-2 organic substances in SI units. *Journal of Physical and Chemical Reference Data*, 11, 1–407.
- Wang, Y., Azais, T., Robin, M., Vallee, A., Catania, C., Legriel, P., Pehau-Arnauudet, G., Babonneau, F., Giraud-Guille, M.M., and Nassif, N. (2012) The predominant role of collagen in the nucleation, growth, structure and orientation of bone apatite. *Nature Materials*, 11, 724–33.
- Wang, Y., Von Euw, S., Fernandes, F.M., Cassaignon, S., Selmane, M., Laurent, G., Pehau-Arnauudet, G., Coelho, C., Bonhomme-Courty, L., Giraud-Guille, M.-M., Babonneau, F., Azais, T., and Nassif, N. (2013) Water-mediated structuring of bone apatite. *Nature Materials*, 12, 1144–1153.
- Wilson, E.E., Awonusi, A., Morris, M.D., Kohn, D.H., Tecklenburg, M.M., and Beck, L.W. (2005) Highly ordered interstitial water observed in bone by nuclear magnetic resonance. *Journal of Bone Mineral Research*, 20, 625–34.
- (2006) Three structural roles for water in bone observed by solid-state NMR. *Biophysical Journal*, 90, 3722–3731.
- Yoder, C.H., Pasteris, J.D., Worcester, K.N., and Schermerhorn, D.V. (2012a) Structural water in carbonated hydroxylapatite and fluorapatite: confirmation by solid state  $^2H$  NMR. *Calcified Tissue Research*, 90, 60–67.
- Yoder, C., Pasteris, J., Worcester, K., Schermerhorn, D., Sternlieb, M., Goldenberg, J., and Wilt, Z. (2012b) Dehydration and rehydration of carbonated fluor- and hydroxylapatite, *Minerals*, 2, 100–117.

MANUSCRIPT RECEIVED NOVEMBER 29, 2017

MANUSCRIPT ACCEPTED JANUARY 9, 2018

MANUSCRIPT HANDLED BY ROBERT HEIMANN